



**HAL**  
open science

## The relationship between eruptive activity, flank collapse, and sea level at volcanic islands: A long-term (>1 Ma) record offshore Montserrat, Lesser Antilles

Maya Coussens, Deborah Wall-Palmer, Peter. J. Talling, Sebastian. F. L. Watt, Michael Cassidy, Martin Jutzeler, Michael A. Clare, James. E. Hunt, Michael Manga, Thomas. M. Gernon, et al.

### ► To cite this version:

Maya Coussens, Deborah Wall-Palmer, Peter. J. Talling, Sebastian. F. L. Watt, Michael Cassidy, et al.. The relationship between eruptive activity, flank collapse, and sea level at volcanic islands: A long-term (>1 Ma) record offshore Montserrat, Lesser Antilles. *Geochemistry, Geophysics, Geosystems*, 2016, 17, pp.2591-2611. 10.1002/2015GC006053 . insu-03581315

**HAL Id: insu-03581315**

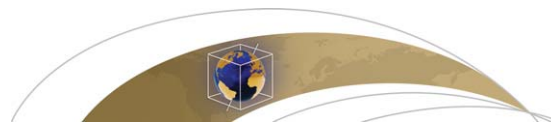
**<https://insu.hal.science/insu-03581315>**

Submitted on 19 Feb 2022

**HAL** is a multi-disciplinary open access archive for the deposit and dissemination of scientific research documents, whether they are published or not. The documents may come from teaching and research institutions in France or abroad, or from public or private research centers.

L'archive ouverte pluridisciplinaire **HAL**, est destinée au dépôt et à la diffusion de documents scientifiques de niveau recherche, publiés ou non, émanant des établissements d'enseignement et de recherche français ou étrangers, des laboratoires publics ou privés.

Copyright



RESEARCH ARTICLE

10.1002/2015GC006053

The relationship between eruptive activity, flank collapse, and sea level at volcanic islands: A long-term (>1 Ma) record offshore Montserrat, Lesser Antilles

Key Points:

- Heightened volcanic activity on Montserrat at 120–190, 760–810, and 900–930 ka
- Large landslides coincide with rapid sea level rise at island arc volcanoes

Supporting Information:

- Supporting Information S1
- Figure S1
- Figure S2
- Table S1
- Table S2
- Table S3

Correspondence to:

M. Coussens,  
mfc1e12@soton.ac.uk,  
maya.pratt@mail.com

Citation:

Coussens, M., et al. (2016), The relationship between eruptive activity, flank collapse, and sea level at volcanic islands: A long-term (>1 Ma) record offshore Montserrat, Lesser Antilles, *Geochem. Geophys. Geosyst.*, 17, 2591–2611, doi:10.1002/2015GC006053.

Received 18 AUG 2015

Accepted 5 JUN 2016

Accepted article online 17 JUN 2016

Published online 16 JUL 2016

Maya Coussens<sup>1</sup>, Deborah Wall-Palmer<sup>2</sup>, Peter. J. Talling<sup>3</sup>, Sebastian. F. L. Watt<sup>2</sup>, Michael Cassidy<sup>4</sup>, Martin Jutzeler<sup>3,5</sup>, Michael A. Clare<sup>3</sup>, James. E. Hunt<sup>3</sup>, Michael Manga<sup>6</sup>, Thomas. M. Gernon<sup>1</sup>, Martin. R. Palmer<sup>1</sup>, Stuart. J. Hatter<sup>1</sup>, Georges Boudon<sup>7</sup>, Daisuke Endo<sup>8</sup>, Akihiko Fujinawa<sup>9</sup>, Robert Hatfield<sup>10</sup>, Matthew. J. Hornbach<sup>11</sup>, Osamu Ishizuka<sup>12</sup>, Kyoko Kataoka<sup>9</sup>, Anne Le Friant<sup>7</sup>, Fukashi Maeno<sup>13</sup>, Molly McCanta<sup>14</sup>, and Adam. J. Stinton<sup>15,16</sup>

<sup>1</sup>School of Ocean and Earth Science, National Oceanography Centre, University of Southampton, Southampton, UK, <sup>2</sup>School of Geography, Earth and Environmental Sciences, Plymouth University, Plymouth, UK, <sup>3</sup>National Oceanography Centre, Southampton, Southampton, UK, <sup>4</sup>Institute of Geosciences, Johannes Gutenberg, University Mainz, Mainz, Germany, <sup>5</sup>Now at University of Tasmania, Hobart, Tasmania, <sup>6</sup>Department of Earth and Planetary, Science University of California, Berkeley, Berkeley, California, USA, <sup>7</sup>Équipe de Géologie des Systèmes Volcaniques, Institut de Physique du Globe de Paris, Sorbonne, Paris Cité, UMR 7154 CNRS, France, <sup>8</sup>Earth Evolution Sciences, University of Tsukuba, Ibaraki, Japan, <sup>9</sup>Research Institute for Natural Hazards and Disaster Recovery, Niigata University, Niigata, Japan, <sup>10</sup>College of Oceanic and Atmospheric Sciences, Oregon State University, Corvallis, Oregon, USA, <sup>11</sup>Institute for Geophysics, University of Texas at Austin, Austin, Texas, USA, <sup>12</sup>Geological Survey of Japan (AIST), Ibaraki, Japan, <sup>13</sup>Earthquake Research Institute, University of Tokyo, Tokyo, Japan, <sup>14</sup>Department of Geology, Tufts University, Lane Hall Medford, Massachusetts, USA, <sup>15</sup>Montserrat Volcano Observatory, Flemmings, Montserrat, <sup>16</sup>Seismic Research Center, University of the West Indies, St. Augustine, Trinidad and Tobago

**Abstract** Hole U1395B, drilled southeast of Montserrat during Integrated Ocean Drilling Program Expedition 340, provides a long (>1 Ma) and detailed record of eruptive and mass-wasting events (>130 discrete events). This record can be used to explore the temporal evolution in volcanic activity and landslides at an arc volcano. Analysis of tephra fall and volcanoclastic turbidite deposits in the drill cores reveals three heightened periods of volcanic activity on the island of Montserrat (~930 to ~900 ka, ~810 to ~760 ka, and ~190 to ~120 ka) that coincide with periods of increased volcano instability and mass-wasting. The youngest of these periods marks the peak in activity at the Soufrière Hills volcano. The largest flank collapse of this volcano (~130 ka) occurred toward the end of this period, and two younger landslides also occurred during a period of relatively elevated volcanism. These three landslides represent the only large (>0.3 km<sup>3</sup>) flank collapses of the Soufrière Hills edifice, and their timing also coincides with periods of rapid sea level rise (>5 m/ka). Available age data from other island arc volcanoes suggest a general correlation between the timing of large landslides and periods of rapid sea level rise, but this is not observed for volcanoes in intra-plate ocean settings. We thus infer that rapid sea level rise may modulate the timing of collapse at island arc volcanoes, but not in larger ocean-island settings.

1. Introduction

Volcanic islands in arc settings grow and decay through eruptive and mass-wasting processes. The rate of island growth reflects the balance of these processes, including the style, composition, and magnitude of individual eruptions [Houghton et al., 1995; Singer et al., 2008; Germa et al., 2010], and variations in the magnitude and frequency of mass-wasting events (e.g., lava dome collapses, flank landslides) [Ablay and Marti, 2000; Cole et al., 2002; Trofimovs et al., 2013]. As a volcanic island grows, the edifice becomes increasingly unstable, resulting in partial flank collapses, which are a ubiquitous feature of composite volcanoes [e.g., Siebert, 1984]. Such collapse events are potential geohazards through the generation of landslides [Siebert, 1984; Watt et al., 2012a,b], and their potential to generate tsunamis [Ward and Day, 2003]. There are few individual volcanic records that span the life cycle of individual composite volcanoes (on the order of 10<sup>5</sup>–10<sup>6</sup> years), but such records can be used to investigate temporal patterns in total volcanic output, and

the relative timing of flank collapses. The instabilities that drive collapses may relate both to internal (e.g., total volcanic output) and external (e.g., eustatic sea level change) processes. To obtain a more complete understanding of the overall controls on volcano growth and destruction, we use a marine stratigraphic record offshore Montserrat to explore patterns of volcanism, sea level change, and flank collapse timing over a  $10^6$  year period.

Here, we use the term flank collapse to refer to gravity-driven failures of volcanic material from subaerial and/or submarine volcanic island flanks, potentially also involving carbonate shelf material. Collapses that only involve material from the carbonate shelf (i.e., generating bioclastic deposits) are referred to as shelf collapses. Flank collapses can involve several cubic kilometers of material, and may or may not be associated with volcanic eruptions. They are distinct from the generally smaller dome collapses, which involve juvenile lava and are a common mass wasting process during the lava-dome forming eruptions that typify volcanism on Montserrat. *Mass-wasting* or *landslides* are used as collective terms here for the different types of collapse events. Landslides may also generate a range of density currents that are represented in the geological record as a variety of density current deposits. In this study, we refer to all submarine density current deposits as *turbidites*, regardless of whether the deposits were generated from fully turbulent or nonturbulent flows.

Triggers of flank or shelf collapses on volcanic islands are poorly understood, but it has been proposed that their frequency is related to eustatic sea level changes, edifice growth, tectonic activity, and rainfall [McGuire et al., 1997; Masson et al., 2006; Sato et al., 2007; Marques et al., 2008; Quidelleur et al., 2008; Hunt et al., 2013, 2014]. Reconstructing prehistorical earthquake and rainfall records are challenging, resulting in difficulties when comparing these potential triggers to landslide occurrence. Previous studies of eustatic sea level change and landslides have been hampered due to difficulties in acquiring sufficient and accurate dates for landslide events. Such studies have typically relied on incomplete information from on-land observations of collapse structures, and/or been restricted to relatively recent events recorded in shallow (<6 m) marine sediment cores and seismic profiles [McMurtry et al., 2004a, 2004b; Boudon et al., 2007; Trofimovs et al., 2013]. Consequently, very few volcanic island landslide events have been dated precisely over time periods that are long enough to include multiple climatic, volcanic, and tectonic cycles [Longpré et al., 2011; Trofimovs et al., 2013; Hunt et al., 2013].

We analyzed Hole U1395B from IODP Expedition 340, drilled in 2012. This Hole is >120 m in length and contains an unusually long (>1 Ma) and detailed marine record of island arc volcanism and mass-wasting activity. Hole U1395B was drilled ~25 km southeast of Montserrat at ~1200 m below sea level (Figure 1), and provides an excellent opportunity to study a long and detailed record of sedimentological processes around an island arc volcano.

The record of marine volcanoclastic deposits (both turbidites and tephra fall deposits) is used as a proxy for volcanic activity at Montserrat. This approach is based on studies of marine deposits associated with the 1995–2010 eruption on Montserrat [Kokelaar, 2002; Trofimovs et al., 2006], which showed that individual pyroclastic flows formed via dome-collapse and explosive eruption events produced widespread volcanoclastic turbidites. We thus expect most volcanoclastic turbidites to represent individual eruptions, but note that some volcanoclastic turbidites may be produced by noneruptive flank collapses, or by reworking of older volcanoclastic deposits. Turbidites from large flank collapses can be identified by their thickness and correlation with debris avalanche deposits (and there are only a few of these around Montserrat) [cf. Lebas et al., 2011], while resedimented turbidites may be more mixed, including bioclastic material. The latter may also still provide a broad proxy for volcanic activity, since they are more likely to be generated during periods of volcanism, when flanks may be destabilized by eruptive activity and deposition of volcanic products [Collins and Dune, 1986; Major et al., 2000; Hunt et al., 2014].

By identifying and dating volcanoclastic deposits from Hole U1395B, we aim to investigate the temporal relationships between mass-wasting, volcanic activity, and sea level over an interval of  $\sim 10^6$  years. This period encompasses a sufficient number of volcanic cycles and eustatic sea level changes to allow for statistically robust hypothesis testing. It is also shown that all of the well-dated major collapse events around Montserrat occurred during periods of rapid sea level rise. We explore whether other volcanic islands (island arcs and intraplate ocean islands) show similar relationships between landslide ages and sea level or volcanism, while noting that many of these landslide ages have considerable uncertainties.

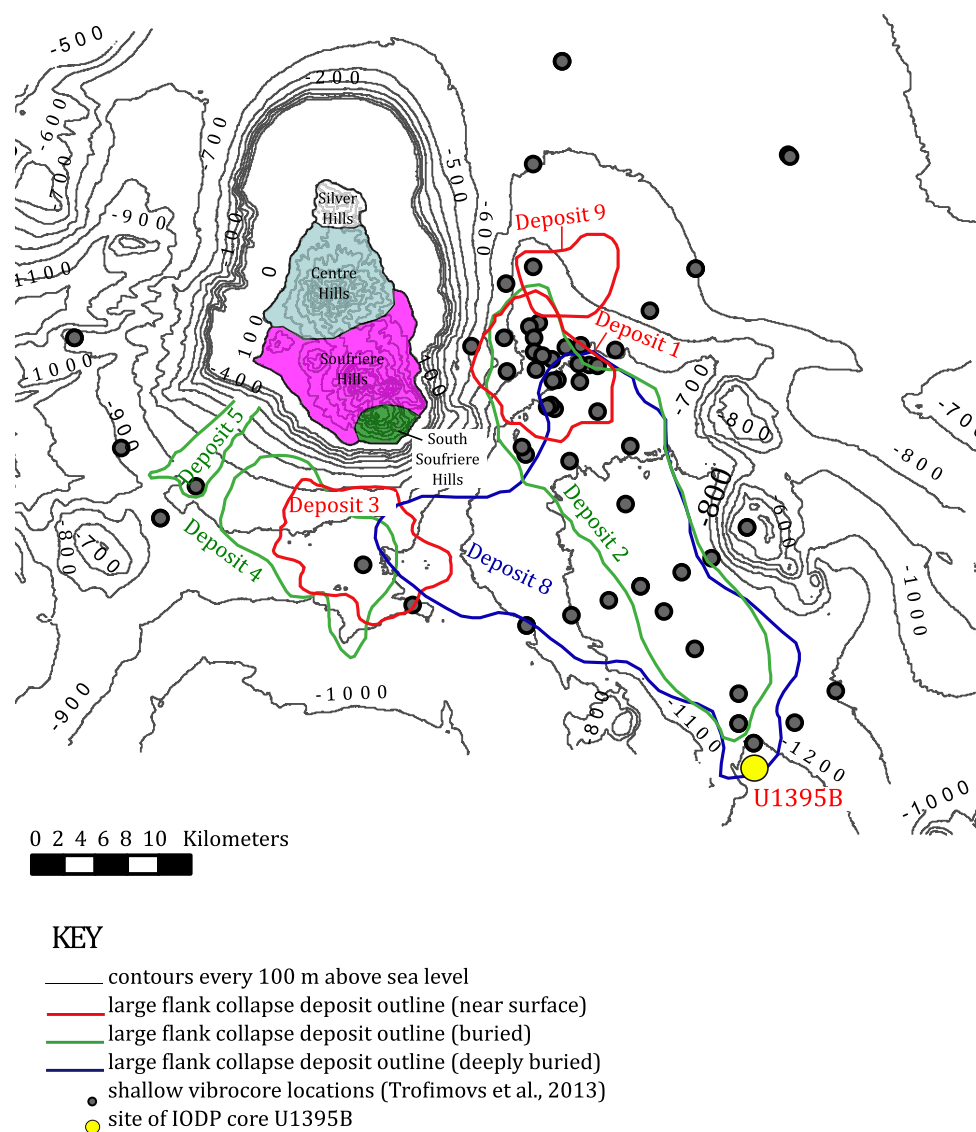


**Figure 1.** Topographic and bathymetric map of Montserrat showing site of U1395B and large debris avalanche flows [Le Friant et al., 2004; Boudon et al., 2007; Lebas et al., 2011; Watt et al., 2012a, 2012b].

## 2. Study Area: Introduction to Montserrat

Montserrat is an island arc volcano located in the Lesser Antilles (Figure 1), which erupted between 1995 and 2010, devastating the city of Plymouth and affecting large parts of the island economy [Kokelaar, 2002; Wadge et al., 2014]. The eruptions included collapse of the active lava dome generating pyroclastic flows and block and ash flows. The largest dome collapse ( $0.21 \text{ km}^3$ ) occurred in 2003 and generated a 0.5–1 m high tsunami on Guadeloupe [Herd et al., 2006; Trofimovs et al., 2008]. Bathymetric mapping has since identified much larger landslide deposits offshore Montserrat with volumes of  $0.3\text{--}20 \text{ km}^3$  [Deplus et al., 2001; Boudon et al., 2007; Lebas et al., 2011; Watt et al., 2012a, 2012b]. Such large landslides have a much higher tsunamigenic potential, and thus represent a more significant hazard than events associated with the recent eruptions.

Since  $\sim 290 \text{ ka}$  (based on subaerial Ar-Ar dates) [Harford et al., 2002], activity at Montserrat has been focused on the andesitic Soufrière Hills volcano, except for a brief interlude of basaltic volcanism at  $\sim 130 \text{ ka}$ , forming the South Soufrière Hills (Figure 1). The previously active volcanic center, at Centre Hills, is dated at 990–

550 ka [Harford *et al.*, 2002]. Between these two periods of activity (550–290 ka), the subaerial record suggests a period of quiescence. The apparent gap in volcanism from 550 to 290 ka is not clear in the marine sediment cores, and the existing subaerial ages may thus reflect a limited stratigraphy represented by on-land exposures, or incomplete study and dating of subaerial outcrops.

The offshore eruption and landslide record around Montserrat has been studied in detail [Deplus *et al.*, 2001; Trofimovs *et al.*, 2006, 2010, 2012, 2013; Boudon *et al.*, 2007; Lebas *et al.*, 2011; Le Friant *et al.*, 2010, 2015; Cassidy *et al.*, 2012b, 2013]. To the southeast and southwest of Montserrat is an extensive shallow core (<6 m) data set (Figure 1). These >80 cores contain hemipelagic sediment and numerous volcanoclastic and bioclastic turbidites from eruption and landslide deposits emplaced during the last ~110 ka [Le Friant *et al.*, 2009; Trofimovs *et al.*, 2010, 2012, 2013; Cassidy *et al.*, 2012b, 2013]. Swath bathymetry and 2-D and 3-D seismic data reveal seven large landslide deposits, dating back to the time of Centre Hills volcanism (Figure 1). These large landslide deposits likely represent flank collapse events as opposed to dome or localized shelf collapses.

It is important to recognize that any study based on a single sampling site will introduce some sampling bias in the record of eruptive and collapse events. The activity at Montserrat is typified by dome-forming eruptions with durations of months to years, interspersed by moderate-sized explosive pulses such as the 1995–2010 eruption [Kokelaar, 2002; Wadge *et al.*, 2014]. Such eruptions form complex volcanoclastic intervals generated by multiple pyroclastic density currents and tephra fall events distributed radially from the volcanic edifice [Trofimovs *et al.*, 2006, 2013; Le Friant *et al.*, 2015]. Hole U1395B is located ~25 km southeast of Montserrat, hence it is only likely to sample mass flows that entered the ocean to the east and south of Montserrat. While some individual events may therefore not be preserved within Hole U1395B, periods of eruption are still likely to be represented, because any one eruption is likely to produce multiple mass flow and tephra fall deposits, with the mass flows, in particular, travelling in a range of directions. For example, the 2003 collapse event (0.1 km<sup>3</sup>) deposited a ~20 cm thick volcanoclastic turbidite at site U1395B [Trofimovs *et al.*, 2008], but small vulcanian eruptions that occurred throughout the 1995–2010 eruption are not represented within Hole U1395B [Kokelaar, 2002; Wadge *et al.*, 2014].

Hole U1395B is only likely to sample a small proportion of tephra fall deposits, as dispersal depends on wind direction and the magnitude of the explosive event. Prevailing wind directions in the troposphere and upper stratosphere are predominantly from the east, and prevailing wind directions in the lower stratosphere are from the west, based on historical data from 1956 to present [Radiosonde wind data, 2012]. Tephra fall deposits may therefore be subject to a spatial sampling bias, with many eruption plumes transported to the west leaving no record within U1395B. However, large explosive eruptions, which can involve multiple phases and be associated with pyroclastic density currents and the generation of offshore turbidites, are still likely to have some representation at the core site as an eruptive event. Because we are interested simply in event timing, rather than magnitude or style, this single core is likely to provide a relatively comprehensive record of eruptions at Montserrat.

### 3. Methods

#### 3.1. Event Deposit Identification

We defined five facies at Site U1395: hemipelagic mud, bioclastic turbidites, mixed bioclastic-volcanoclastic turbidites, volcanoclastic turbidites, and tephra fall deposits (Figure 2). Hemipelagic mud is mostly composed of carbonate and detrital clay with abundant interspersed foraminifera. The volcanoclastic turbidite and tephra fall deposits are less easily distinguished from each other, as both can comprise normally graded sand and silt [Trofimovs *et al.*, 2013]. Their discrimination requires grain size and component analysis to identify the type of event deposit [Cassidy *et al.*, 2014, 2015].

Tephra fall layers were defined in this study as having <30% bioclasts, a Folk and Ward [1957] sorting coefficient of <0.5 phi (where grainsize (phi) =  $-\log_2$  (grain size (mm))) (analyses conducted on particles from  $-1$  to 9 phi), and a thickness of <20 cm. Tephra fall deposits are well sorted by density and dominated by volcanic clasts. Hole U1395B is ~25 km away from Montserrat, where tephra fall deposits from moderate-sized explosive eruptions, even downwind, are likely to be a few centimeters thick; consequently, thick (>20 cm) deposits are unlikely to represent tephra fall layers. Large magnitude eruptions are rare within the Lesser Antilles [Palmer *et al.*, 2016]. Thin tephra fall layers are commonly mixed with surrounding

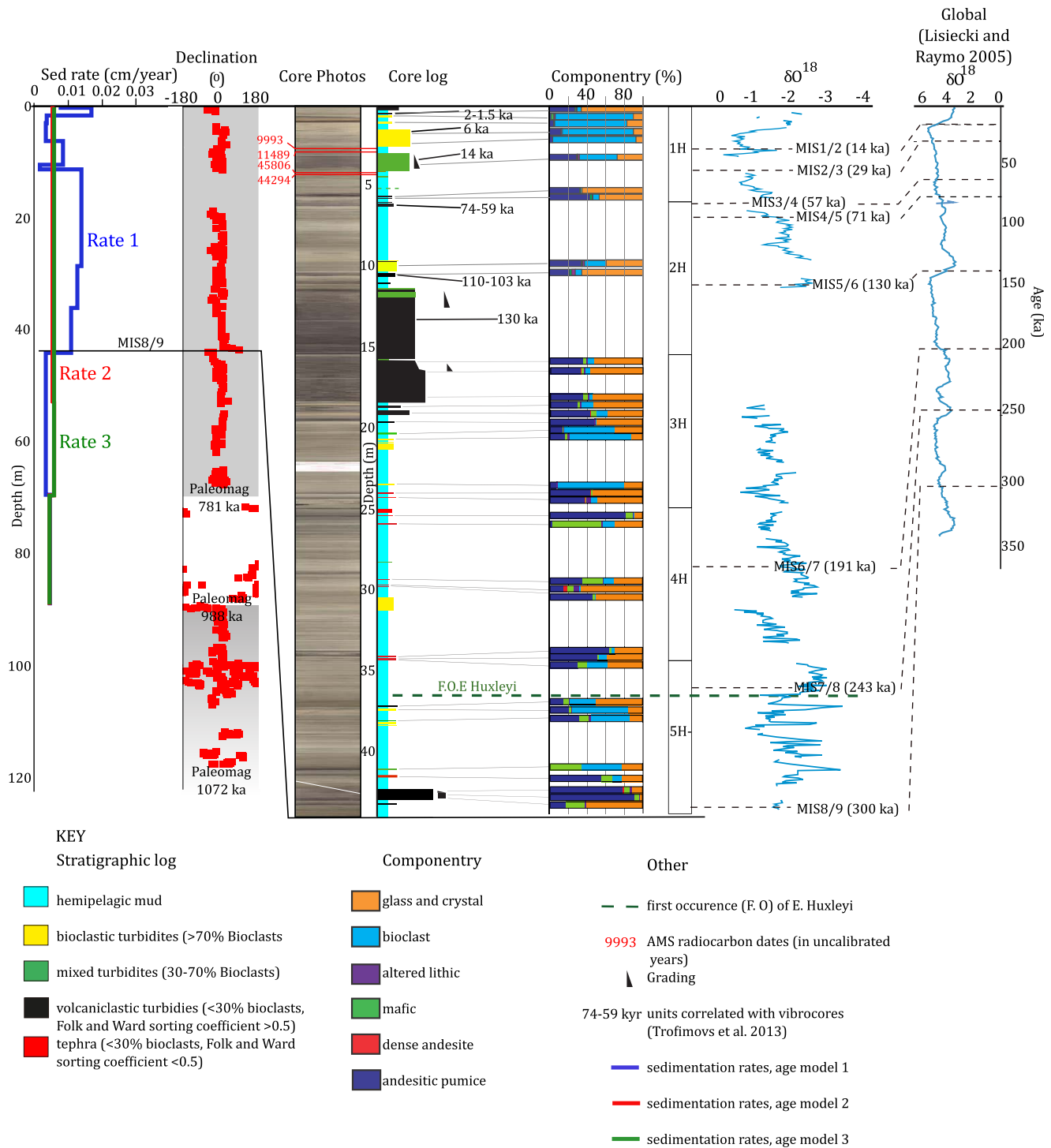


**Figure 2.** Upper 44 m of Hole U1395B including core log and photos; calculated sedimentation rates for all age models; NRM declination data from shipboard measurements; section of stratigraphic core photos and log; sample of componentry data; oxygen isotopes from this study and the global oxygen isotope curve from *Lisiecki and Raymo* [2005]. For full componentry data and stratigraphic log of Hole U1395B, see supporting information data.

hemipelagic material, through bioturbation, bottom current reworking, or disturbance during coring, thus artificially increasing their apparent bioclast content. We thus examined the core for any evidence of post-depositional processes (supporting information Figure S1) and have defined tephra fall layers as comprising <30% bioclast content to allow for postdepositional mixing. Volcaniclastic turbidites are deposits from high-energy, erosive flows that may entrain bioclastic material and preexisting volcaniclastic sediments.

**Table 1.** AMS Carbon Dates From Core U1395

Allocation Number	Publication Code	Sample Identifier	$\delta^{13}\text{C}_{\text{VPDB}}\text{‰} \pm 0.1$	Carbon Content (% by wt.)	$^{14}\text{C}$ Enrichment (% Modern)	$\pm 1\sigma$ (% Modern)	Conventional Radiocarbon Age (Years BP)	$\pm 1\sigma$ (Radiocarbon Years BP)	Stratigraphic Position (cm)
1721.0513	SUERC-46961	1H2W-108-110	1.1	10.9	28.82	0.13	9,993	37	258–260
1721.0513	SUERC-46962	1H2W-115-117	1.1	10.8	23.93	0.12	11,489	40	265–267
1721.0513	SUERC-46965	1H3W-109-111	1.2	11.4	0.33	0.06	45,806	1,463	409–411
1721.0513	SUERC-46966	1H3W-116-118	1.0	11.3	0.40	0.06	44,294	1,208	416–418

Therefore, although some parts of a volcanoclastic turbidite can be well-sorted, they are likely to be less well sorted than tephra fall deposits [Cassidy *et al.*, 2014]. Volcanoclastic turbidites are defined here as comprising <30% bioclasts, with a Folk and Ward [1957] sorting coefficient >0.5 ( $\phi$ ). Mixed turbidites are defined as having 30–70% bioclasts. Bioclastic turbidites are defined as containing >70% bioclasts (see supporting information Figures S1–S3).

Grain size measurements using laser-diffraction analyses were carried out using a Malvern Master-sizer 2000 particle size analyzer, which can measure grain sizes between 0.2 and 2000  $\mu\text{m}$ . To disperse grains, 25 ml of reverse osmosis water with 0.05% sodium hexametaphosphate dispersant was added to 1  $\text{cm}^3$  of sample and left overnight on a shaking table. Samples were analyzed in triplicate and accuracy was monitored using standard size particles (32 and 125  $\mu\text{m}$ ) [see Hunt *et al.*, 2013 for details]. Componentry analysis was conducted on sieved fractions >63  $\mu\text{m}$  and <250  $\mu\text{m}$  material from all volcanic-rich units and some bioclastic-rich units. For each sample, approximately 400 grains were point-counted using an area counting method. Componentry classes follow Le Friant *et al.*, [2008] and Cassidy *et al.*, [2014]: (1) vesicular pumice clasts; (2) nonvesicular andesite; (3) altered lithic clasts; (4) crystal and glass fragments; (5) mafic scoria clasts; and (6) bioclasts. Grain size and componentry data are summarized in supporting information Tables S1 and S2, respectively (see supporting information Figures S1–S3 for photos).

### 3.2. Dating Hole U1395B

The core from U1395B core was dated using a combination of oxygen isotope stratigraphy, biostratigraphy, AMS radiocarbon dating, and the shipboard paleomagnetic reversal records. Higher-resolution dating was carried out on the upper 40 m of Hole U1395B using oxygen isotope stratigraphy of the hemipelagic mud (Figure 2). Twenty *Globigerinoides ruber* specimens between 250 and 355  $\mu\text{m}$  in size were picked and analyzed from each hemipelagic sample. Samples were 7 cm apart and analyzed at Plymouth University on an Isoprime Instruments continuous flow mass spectrometer with a Gilson Multiflow carbonate autosampler. Oxygen Isotope values are given as deviations in the isotope ratios ( $^{18}\text{O}/^{16}\text{O}$ ) per mil (‰), using the VPDB scale (supporting information Table S3).

To limit the ambiguity of identifying marine isotope stages, biostratigraphic boundaries and AMS radiocarbon dates (for sediments <50 ka) were used (Table 1).

Calcareous nannofossils in the <63  $\mu\text{m}$  material from hemipelagic samples were analyzed using scanning electron microscopy (SEM), employing the calcareous nannofossil zonation of Kameo and Bralower [2000] for the Caribbean Sea. Sediment was fixed to metal stubs using a thin layer of spray adhesive, then sputter-coated with gold. The first occurrence of *Emiliania huxleyi* (250 ka) was found at 36.74 m, close to the MIS 7/8 boundary (243 ka). The first occurrence of *E. huxleyi* has also been identified across the MIS 7/8 transition in Hole U1396C [Wall-Palmer *et al.*, 2014] and CAR-MON 2 [Le Friant *et al.*, 2008] (Figure 3).

New AMS dates were obtained in this study from four samples in the upper 4 m of Hole U1395B (aged <57 ka), in addition to the radiocarbon AMS dates reported by Trofimovs *et al.*, [2013]. Approximately 1000 pristine tests of white *Globigerinoides ruber* >150  $\mu\text{m}$  in size were picked (~17 mg) and then sonically cleaned. The new samples were located beneath two of the largest turbidites (Figure 3). Radiocarbon dates were measured at Scottish Universities Environmental Research Council (SUERC) using their in-house protocol [see Trofimovs *et al.*, 2013].

Paleomagnetic reversals were determined on board during Expedition 340 as 180° changes in declination (after azimuthal correction). Associated changes in inclination after demagnetization of the natural remnant magnetization (NRM) in a field of 20 mT (to remove the coring overprint) were also recorded [see Hatfield and Expedition 340 Scientists 2013 for details]. Here we report ages based on the geomagnetic polarity

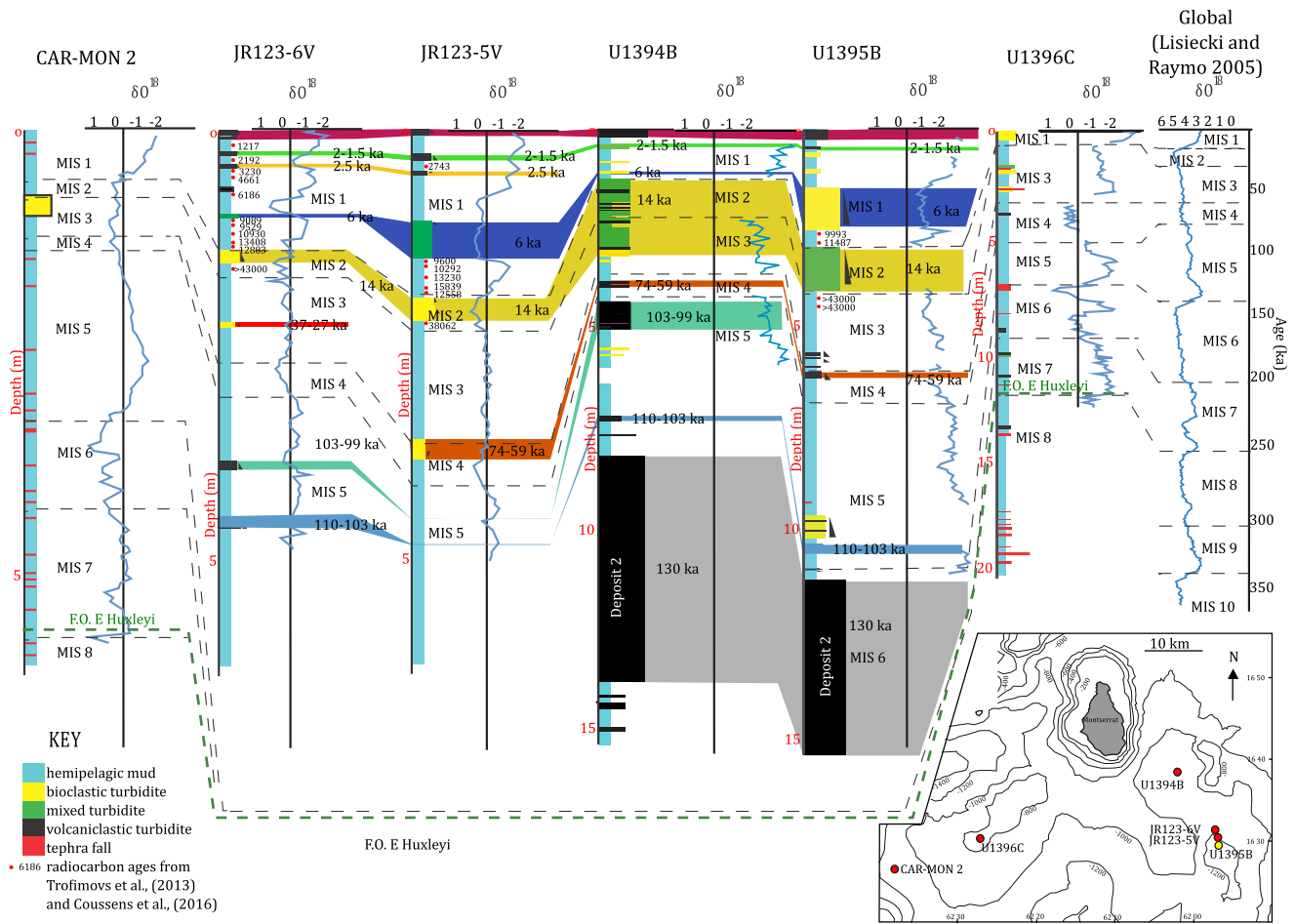


**Figure 3.** Correlations of the top of core U1395B with shallow cores based on componentry and oxygen isotope data [Le Friant et al., 2008; Cassidy et al., 2012b, 2013; Ogg, 2012; Trofimovs et al., 2013; Wall-Palmer et al., 2014].

timescale (GPTS) of Ogg [2012] instead of the GPTS of Cande and Kent [1995] as was reported on board the ship. Two paleomagnetic reversals occur at 781 ka (6.3% error) and 988 ka (11.3% error) in core U1395B [Cande and Kent 1992a, 1992b; Ogg, 2012], with a possible third reversal at the base of the core at 1072 ka (11.3% error) [Cande and Kent, 1992; Ogg, 2012]. The 781 ka reversal is obscured by a volcanoclastic turbidite and coring disturbance at 68.5–71 m (Figure 2). The coring disturbance occurs primarily within the volcanoclastic turbidite. The reversal is likely to have occurred shortly prior to the emplacement of the volcanoclastic turbidite, thus obscuring the reversal through erosion of hemipelagic mud. Here we take the base of the volcanoclastic turbidite as 781 ka. The MIS 8/9 (300 ka) boundary is interpreted to occur at ~44 m, suggesting that sedimentation rates decrease with depth in the core. The 988 ka reversal occurred between 88.3 and 89.9 m with a midpoint at 89.1 m (Figure 2). The 1072 ka reversal may be present at the base of Hole U1395B (Figure 2) but this is less certain due to poor sample recovery at the base of the core.

Data from Hole U1395B were also compared and correlated to previously studied cores around Montserrat (Figure 3). These cores include JR123-5V, JR123-6V, CAR-MON 2, and Hole U1396C (Figure 3). JR123-5V and JR123-6V are part of an extensive vibrocore data set that has been used to compile a comprehensive stratigraphy of Montserrat over the past 110 ka [Trofimovs et al., 2013]. The vibrocore data set includes over 80 <6 m long cores with 40 accelerator mass spectrometry (AMS) radiocarbon dates (Figure 3). JR123-5V and JR123-6V are located 1–2 km north of Site U1395, and some units within core U1395B can be correlated to units found in JR123-5V and JR123-6V by age (Figure 3). CAR-MON 2 is a piston core collected in 2002, which extends 5.75 m and was taken ~55 km to the southwest of Montserrat (Figure 3) [Le Friant et al., 2008]. Site U1396C is situated ~33 km southwest of Montserrat (Figure 3) and was collected during IODP Expedition 340 [Wall-Palmer et al., 2014].

## 4. Results

Hole U1395B is 127.51 m long and it is composed of 62.6% hemipelagic mud, 24.4% volcanoclastic deposits, 9% mixed turbidites, and 4% bioclastic deposits, by deposit thickness. The core comprises 18 bioclastic turbidites, 48 tephra fall deposits, 26 mixed turbidites, and 41 volcanoclastic turbidites. Core recovery is good (>90%), with only one occurrence of basal flow-in coring disturbance over the studied core length at the bottom of Core U1395B-2H, followed by probable fall-in at the top of Core Section U1395B-3H [Jutzeler *et al.*, 2014].

### 4.1. Age Models

Unit ages have been estimated by calculating hemipelagic sedimentation rates between dated horizons, assuming constant sedimentation rates between dated horizons. Developing accurate age models for marine cores are difficult due to the effects of erosion (commonly at the base of turbidites), short-term fluctuations in sediment supply, and the sometimes ambiguous identification of marine isotope stages. We therefore include three age models to help capture these uncertainties, and their implications.

Age models can be affected by erosion. In the upper 5 m of U1395B, ~88 cm of hemipelagic sediment may have been eroded by the 12–14 ka turbidite [Trofimovs *et al.*, 2013], indicating that the effects of erosion at Site U1395B may be significant. Erosion rates in the upper 10 m of U1395B are well constrained by a combination of AMS dates from this study, and correlation with well-dated units (40 AMS dates) in the shallow vibrocore data set [Trofimovs *et al.*, 2013]. Below the threshold for AMS radiocarbon dating (>10 m in Hole U1395B), the effects of erosion by turbidites cannot be accurately constrained at site U1395B, potentially leading to inaccuracies in age models. It is likely that most turbidity currents are erosive, removing underlying hemipelagic mud and event deposits from the stratigraphy resulting in the underestimation of the true sedimentation rate. We expect this to be a systematic error affecting the whole core, however, rather than something that introduces bias to specific time periods.

Dating cores using oxygen isotopes may also lead to age model inaccuracies due to difficulties in identifying marine isotope stages (MIS). Oxygen isotopes from Hole U1395B have been compared to the Lisiecki and Raymo [2005] curve; but, local factors may affect the magnitude of isotope fluctuations and erosion may remove parts of the isotope record, resulting in the misidentification of MIS boundaries. Any inaccuracies in the age models used will affect the reliability of unit ages assigned to individual events, and thus affect subsequent analysis of the data set.

Assuming that the average total erosion beneath turbidites is on the order of centimeters, and assuming that MIS boundaries have been correctly constrained within a few centimeters, the event dating errors are likely to be on the order of  $10^2$ – $10^5$  years. This is of a similar magnitude to stratigraphic gaps identified in other cores around Montserrat, including instances where >30 ka of stratigraphy was removed by turbidite erosion (JR 123-5-V and Hole U1396C) [Trofimovs *et al.*, 2013; Wall-Palmer *et al.*, 2014]. In order to assess how sensitive our event-frequency analysis is to dating errors of this magnitude, we conduct the same analysis with three different age models. Age Model 1, described below, uses all age constraints (i.e., MIS boundaries, paleomagnetic reversals etc.) but is also potentially more susceptible to the effects of erosion, producing a record with apparent fluctuations in sedimentation rate. Age Models 2 and 3 use fewer age constraints, resulting in a smoother estimate of long-term sedimentation rate that may be more geologically realistic. Individual unit ages derived from the three age models may vary by up to  $10^5$  years. By using all three age models within subsequent analyses, we can test how robust our results are to these uncertainties.

#### 4.1.1. Age Model 1

This model uses 11 dated horizons, including horizons derived from correlations to units described in Trofimovs *et al.* [2013], identification of MIS boundaries, and identification of paleomagnetic reversals. The 2–1.5, 6, 14, 74–59, 110–103, and 130 ka deposits from Trofimovs *et al.* [2013] and Cassidy *et al.* [2013] have been correlated to units in U1395B. Unit ages of 1.75, 6, 14, 66.5, 107, and 130 ka in Hole U1395B at core depths of 0.49, 2.52, 3.98, 6.26, 10.47, and 18.49 m, respectively, were used in age model 1. Using oxygen isotope analysis, three MIS boundaries were identified and used. These are MIS boundaries 6/7 (191 ka), 7/8 (243 ka), and 8/9 (300 ka) at core depths of 28.31, 35.93, and 43.84 m, respectively [Lisiecki and Raymo, 2005]. Finally, two paleomagnetic reversal dates of 781, and 988 ka, at depths of 63.06, and 89.08 m are used in age model 1.

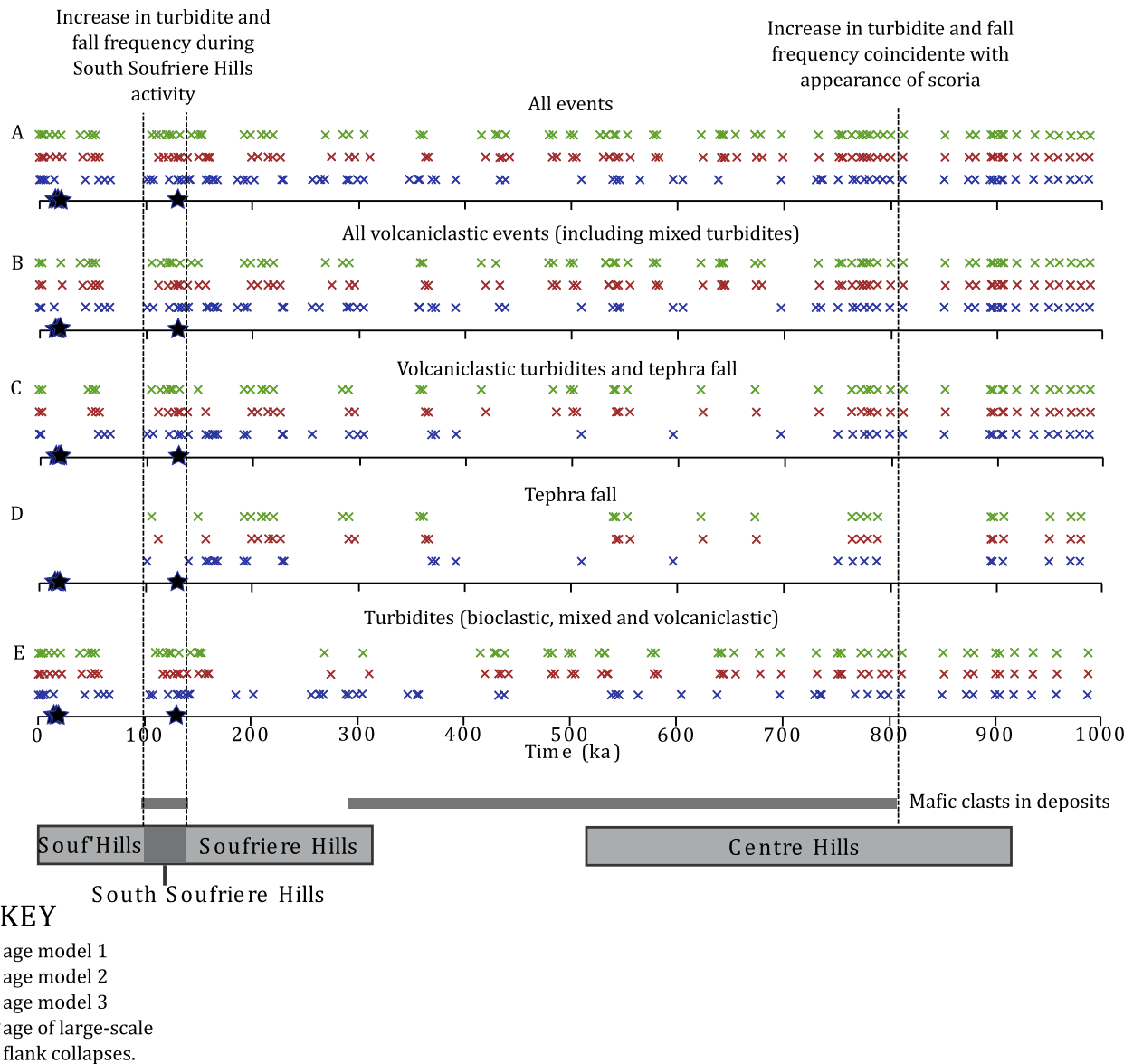


**Figure 4.** Timing of (a) all events, (b) volcanoclastic events (tephra fall and turbidite deposits; including mixed composition turbidites), (c) volcanoclastic events (tephra fall and volcanoclastic turbidite), (d) tephra fall deposits, and (e) all turbidites at Montserrat. In each case, three different age models are shown. Age model 1 (green) uses oxygen isotope data, biostratigraphic data, AMS dates, and paleomagnetic dates. Age model 2 (red) uses Deposit 2 as a boundary at 130 ka (Figure 2), and the paleomagnetic intervals. Age model 3 (blue) uses only the paleomagnetic data. Clustering of events in all age models can be seen at ~950–860, 810–750, 200–100, and from ~50 ka, on Montserrat. There is an absence of prolonged pauses in activity. Thin grey lines show occurrence of scoria within core U1395B, the thick grey line shows known extents of activity at volcanic centers on Montserrat based on limited subaerial dating [Harford et al., 2002].

Using Age Model 1, the calculated sedimentation rates in the upper 300 ka of Hole U1395B fluctuate between 2 and 17 cm/ka, and encompass the range of hemipelagic sedimentation rates (5–10 cm/ka) previously determined in the area [Reid et al., 1996; Watt et al., 2012b]. The greater variability in apparent accumulation rates determined from Age Model 1 (particularly for the lower sedimentation rates) likely reflects the effects of turbidite erosion. Sedimentation rates in age model 1 between 300 and 988 ka are relatively constant at 3.2–9 cm/ka. The reduction in variability of sedimentation rates further down the core likely reflects the fact that there are fewer dated horizons deeper in Hole U1395B, resulting in a smoother apparent sedimentation rate.

**4.1.2. Age Models 2 and 3**

Age Model 2 uses Deposit 2 as a boundary at 130 ka (Figure 2) [Cassidy et al., 2015] at 18.49 m, and the paleomagnetic dates of 781, and 988 ka, at depths of 63.06 m, and 89.08 cm, respectively. Age Model 3 uses

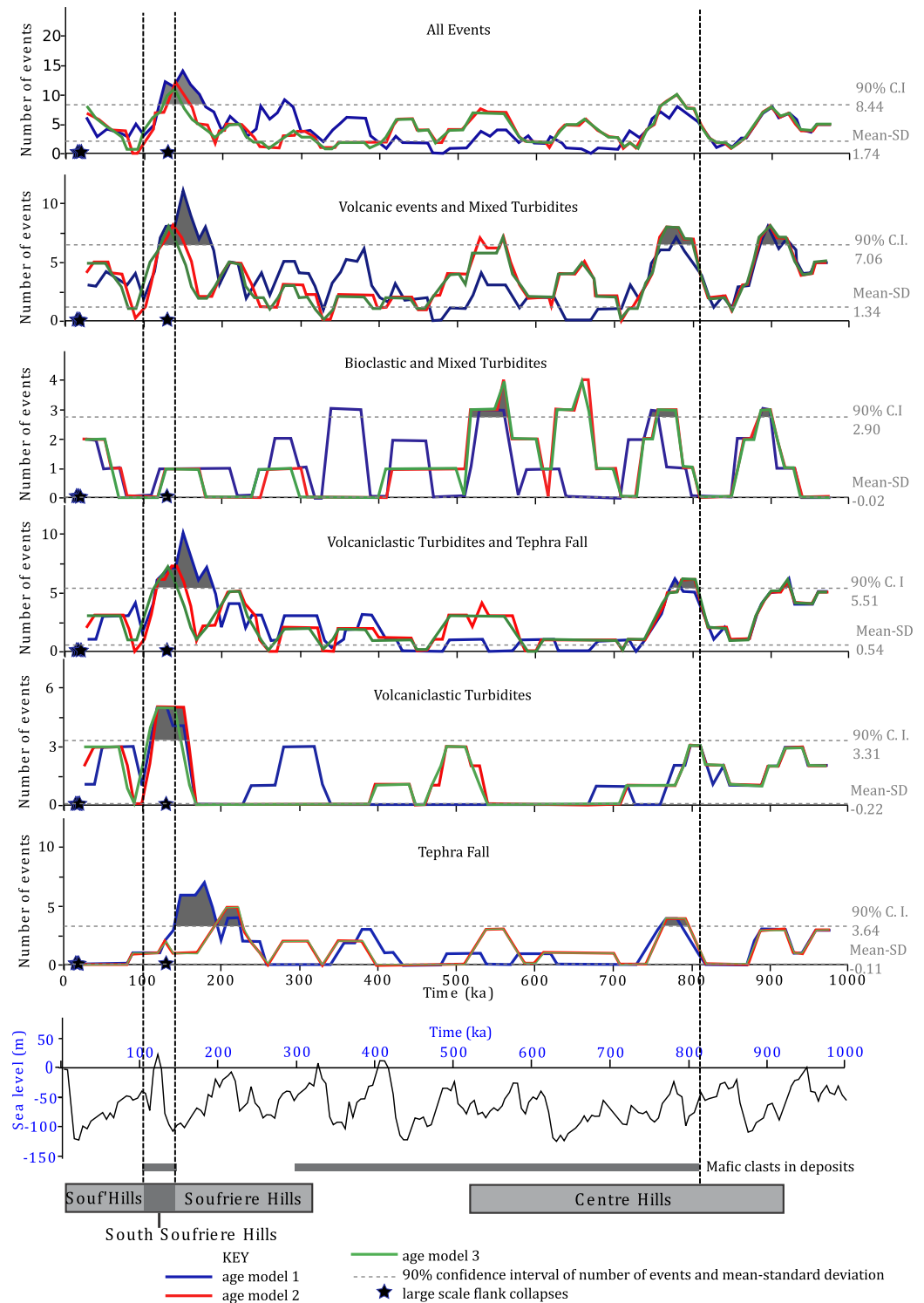


**Figure 5.** Number of events within 50 kyr (centered on window, at 10 kyr increments). Peaks correspond to clusters in Figure 4. Age model 1 (green) uses oxygen isotope data, biostratigraphic data, AMS dates, and paleomagnetic dates. Age model 2 (red) uses Deposit 2 as a boundary at 130 ka (Figure 2), and the paleomagnetic intervals. Age model 3 (blue) uses only the paleomagnetic data. Peaks in event frequency occur at ~930 to ~900 ka, ~810 to ~760 ka, and ~190 to ~120 ka. Periods when event frequency is above the 90% confidence interval in all age models are shaded in grey. The black line is the Miller *et al.*, [2005] sea level curve in meters from present-day sea level. Thin grey lines show occurrence of mafic scoria within Hole U1395B, the thick grey line shows known extents of activity at volcanic centers on Montserrat based on limited subaerial dating [Harford *et al.*, 2002]. There is a peak in event frequency that coincides with the appearance of mafic scoria in Hole U1395B and all large flank collapses occur during periods of rapid sea level rise.

**Table 2.** Results of Linear Statistical Tests for Turbidite Frequency and Sea Level Correlations<sup>a</sup>

	Age Model 1	Age Model 2	Age Model 3
Linear model	0.0898	<i>0.00176</i>	<i>0.00285</i>
Generalized linear model	0.083407	<i>0.00138</i>	<i>0.00696</i>
Proportional hazards model	0.106	<i>0.00219</i>	<i>0.00942</i>

<sup>a</sup>Italicized values show when statistical tests are significant, (i.e., when the null hypothesis can be rejected).

only the two paleomagnetic dates. Using Age Models 2 and 3, estimated sedimentation rates are less variable throughout the core with long-term rates of 4–8 cm/ka.

#### 4.2. Event Frequency Offshore Montserrat

Events are not distributed regularly through time in core U1395B, but appear to cluster within specific time periods (Figure 4). To better understand this long-term variation in event timing we conduct a moving sum, where the number of events are summed every 50 kyr, at 10 kyr increments. Observations do not change when using bins of 30 and 100 kyr (see supporting information Figures S4 and S5). Conservatively, we classify periods of increased frequency as periods where all three age models show that the frequency of event deposits is above the mean 90% confidence interval of the moving sum data (Figure 5). Periods of reduced activity are defined as periods where all three age models show that event frequency is below 1 standard deviation from the mean. In all age models, these periods of relative quiescence last on the order of  $10^4$ – $10^5$  kyr. In Hole U1395B, all age models show an increased frequency of all event deposits (above the 90% confidence interval of 8.44 events in 50 ka) between  $\sim 170$  and  $\sim 120$  ka. This peak in Montserrat's volcanism lies within the period of Soufrière Hills activity (constrained from subaerial dates as 290 ka to present, but see discussion in section 5.1), and suggests that the largest flank collapse of Soufrière Hills (Deposit 2, at 130 ka) and the South Soufrière Hills basaltic episode ( $\sim 130$  ka) both occurred toward the end of the most active phase of Soufrière Hills' eruptive history.

When examining volcanoclastic deposits only (volcanic turbidites and tephra fall), there are three periods where frequency is greater than the mean 90% confidence interval, between  $\sim 930$  to  $\sim 900$  ka,  $\sim 810$  to  $\sim 760$  ka, and  $\sim 190$  to  $\sim 120$  ka. We interpret periods with a higher frequency of both tephra fall and volcanoclastic turbidites as representing episodes of elevated eruptive activity at Montserrat (Figure 5). The older two periods coincide with activity at Centre Hills volcano, and the younger period (which is similar to that derived from the whole data set) to Soufrière Hills.

The periods of heightened volcanic activity show a general correlation with changes in the style of eruptions at Montserrat (Figures 4 and 5). The  $\sim 810$  to  $\sim 760$  ka increase in event frequency coincides with the appearance of scoria within Hole U1395B. The  $\sim 190$  to  $\sim 120$  ka increase in event frequency coincides broadly with the onset of activity at South Soufrière Hills [Harford *et al.*, 2002].

To test if there is any correlation between sea level and turbidite frequency, we use a linear model (LM), generalized linear model (GLM), and proportional hazards model (PHM) after binning the data into 10 kyr intervals. For further details on the statistical methods, see Hunt *et al.* [2014] and Clare *et al.* [2016]. Unit ages are given in supporting information Table S4 and test results are given in Table 2.

Statistical analyses are conducted on all three age models in order to test the sensitivity of results to dating errors and to determine if the results are artefacts of the specific age model used. By comparing results from the three age models, the effects of age uncertainty can be better understood. We pose the null hypothesis that turbidite frequency is not correlated with sea level, and  $p$ -values  $< 0.05$  allow us to reject this hypothesis. Table 2 shows that using age model 1 does not show significance in any statistical tests, but using age models 2 and 3 shows significance in all three statistical tests. It should be noted, however, that the correlation coefficient for LM is very low (0.002, 0.085, and 0.077 for age models 1–3, respectively). Low correlation coefficients for age models 2 and 3 indicate that while there may be a broad correlation between sea level and turbidite frequency, the variation means that the scatter about that trend is very wide. Grouping together of turbidites from eruptive and collapse activity, effects of data binning, or genuine natural noise, may cause this broad scatter. We therefore conclude that all three age models are in agreement and show that there is little to no correlation between sea level and turbidite frequency. Dating errors are unlikely to affect this observation due to the consistency of this result across all three age models.

Although there appears to be no correlation between turbidite frequency and sea level, all three of the dated larger landslide deposits from Soufrière Hills volcano (Deposits 1 and 5, 8–14 ka and Deposit 2, 130 ka occur during periods of rapid sea level rise ( $>5$  m/ka) (Figure 5). Note that older landslides of Center Hills age are not well dated. Larger landslide deposits, associated with volcanic flank collapse, are easily distinguishable from other eruption-related deposits, unlike turbidites, and there is a better degree of confidence in the dating of these events. We investigate this apparent correlation in a later section using a wider global data set (section 5.5.).

## 5. Discussion

### 5.1. How Does the Submarine Record Relate to Subaerial Activity?

Montserrat is part of an active island arc with numerous active volcanoes on other islands, which may be the source of some deposits in the U1395B stratigraphy. For example, site U1395B is situated  $\sim 25$  km south-east of Montserrat and  $\sim 35$  km downwind (northwest) of Guadeloupe [*Radiosonde wind data*], which is thus also a plausible potential source for deposits in the core. Eruptive products from Guadeloupe can be distinguished using lead isotopes because Guadeloupe has a higher radiogenic lead component [*Cassidy et al., 2012a; Palmer et al., 2016*], and *Coussens et al.* [2016] use Pb isotopes to show that most tephra layers recorded within Hole U1395 B are likely to be from Montserrat. Over the past 1 Ma [*Samper et al., 2007*], volcanic activity occurred in the southeast of Guadeloupe at Grande Découverte Soufrière, producing landslides that have mostly traveled westward into a canyon system [*Samper et al., 2007*]. The canyon system has accumulated deposits toward the west or southwest of Guadeloupe: thus, landslides and turbidites from Guadeloupe are unlikely to produce deposits within Hole U1395B, and we assume that the majority of visible turbidite layers are from Montserrat.

Limited Ar-Ar dating from on-land samples on Montserrat suggests that volcanism occurred at Center Hills between  $\sim 990$  and 550 ka [*Harford et al., 2002*] followed by a long hiatus in activity until  $\sim 290$  ka, when activity commenced at Soufrière Hills. At  $\sim 130$  ka there was a brief period ( $\sim 10$  kyr) of eruptive activity at the new volcanic center, South Soufrière Hills, after which activity migrated back to the Soufrière Hills. The apparent gap in subaerial volcanism from  $\sim 500$  to 290 ka is not replicated in any of the age models for Hole U1395B (Figures 4 and 5), where the periods of relative quiescence are much shorter, lasting  $10^4$ – $10^5$  kyr. This suggests that activity migrated relatively rapidly between Centre Hills and Soufrière Hills, and may even have overlapped. This difference between the subaerial and marine records is likely an artifact of limited dating, exposure, and erosion of the subaerial record. As such, the offshore stratigraphy provides a higher resolution record and a better means of investigating temporal patterns in volcanic activity in greater detail.

*Trofimovs et al.* [2006] showed that 90% of the eruptive products from the 1995–2010 eruption of Montserrat had been deposited offshore, supporting our inference that the submarine record is likely to provide a more complete archive of events than the subaerial record. However, deposition in marine settings involves complex transitions between subaerial and submarine transport processes. Thus, although the offshore stratigraphy records more volcanic events than the subaerial record, offshore facies may not provide a truly representative record of a particular type of eruption.

### 5.2. How Does the Frequency of Collapses Relate to Volcanism?

Increases in the frequency of tephra fall deposits above the mean 90% confidence interval (3.64 events in 50 ka) indicate that there was more explosive volcanic activity between  $\sim 800$  to  $\sim 760$  ka (Centre Hills period), and  $\sim 230$  to  $\sim 140$  ka (Soufrière Hills period) (Figure 5). Turbidite frequency also increases during these periods, but not all observed increases are above the mean 90% confidence interval (Figure 5). These observations are consistent for all age models used, suggesting that these periods of increased volcanism and turbidite frequency are unlikely to be age model artefacts. During periods of effusive volcanic activity (i.e., the lava-dome forming eruptions that typify much of Montserrat's volcanism), there is a greater rate of edifice growth and an increase in the number of volcano-tectonic earthquakes and explosive eruptions, all of which are likely to enhance the likelihood of mass wasting. The largest flank collapse from Soufrière Hills (130 ka) occurred near the end of the peak activity at the center (whether derived from all core deposits, or tephra fall deposits alone), suggesting that elevated output at this time led to major flank instability.

Bioclastic turbidites show another increase in frequency at  $\sim 560$  to  $\sim 500$  ka suggesting that other factors may be important in triggering or priming carbonate shelf collapse (Figure 5), such as sea level change or large earthquakes.

### 5.3. How Does the Frequency of Collapses at Montserrat Relate to Sea Level?

Turbidite frequency does not show a statistically robust correlation with eustatic sea level changes (in all age models), but all three of the well-dated large-scale landslides ( $>0.3$  km<sup>3</sup>) from Montserrat (Deposits 1, 2, and 5) occurred during periods of rapid ( $>5$  m/ka) global sea level rise (Figure 5) [Miller *et al.*, 2005]. Deposits 1 and 5 (dated between 14 and 8 ka) coincide with rapid sea level rise at 15–5 ka, from 60 to 1.6 m below present-day sea level (Figure 5). Deposit 2 is dated at 130 ka, which coincides with a second period of rapid sea level rise at 130–120 ka (Figure 5). Although this is a small number of events, the record suggests that rapid sea level rise may trigger or precondition the flank collapses on Montserrat.

### 5.4. Large-Scale Flank Collapse: Constructing a Global Landslide Record

To investigate if large landslide occurrences during rapid sea level rise are replicated more widely, we have compiled a global data set of landslide ages at volcanic islands over the past 1 Ma, building on the compilation by Quidelleur *et al.*, [2008]. The compiled global data set has 25 ages from volcanic islands (errors  $< \pm 22.5$  ka) that are constrained within errors of  $\pm 22.5$  ka, comprising 9 from ocean islands and 16 from island arcs (Tables 3 and 4).

Many landslides have large age uncertainties, and if age errors are too large (i.e., on the order of sea level cycles) then relationships between sea level, volcanism, and landslides cannot be determined [Pope *et al.*, 2015]. Our age-uncertainty criterion of  $< \pm 22.5$  ka has been selected on this basis, because it provides a sufficiently large data set to observe potential patterns, with age errors that are a similar order of magnitude to the periodicity of sea level cycles ( $10^3$ – $10^4$  years).

#### 5.4.1. Ocean Islands

Multiple large-scale landslide deposits dating back to at least 22 Ma lie offshore the Canary Islands [Stillman, 1999]. The oldest well-dated landslide from the island of El Hierro is El Julan, to the SW (130 km<sup>3</sup>) [Gee *et al.*, 2001a, 2001b]. Onshore there is an 8 km wide scar, with infilling material dated at  $< 158 \pm 4$  ka [Guillou *et al.*, 1996]. Turbidite P, in the Madeira Abyssal Plain, is dated at  $540 \pm 10$  ka using biostratigraphy, and is correlated to the El Julan landslide based on geochemistry and subaerial date constraints [Hunt *et al.*, 2013], and is our best age estimate of the El Julan collapse. North of El Hierro lies the El Golfo deposit (150 km<sup>3</sup>) [Urgeles *et al.*, 1997], which is correlated with a large (14.5 km wide) subaerial crater [Urgeles *et al.*, 1997]. This scar is dated between  $87 \pm 8$  ka and  $11 \pm 7$  ka using Ar-Ar dating of material that are incised by and infill the scar [Guillou *et al.*, 1996]. In the Madeira Abyssal Plain, turbidite B is correlated with the El Golfo collapse [Hunt *et al.*, 2013] and is dated at  $15 \pm 5$  ka [Weaver *et al.*, 1992; Hunt *et al.*, 2013] using biostratigraphy of surrounding hemipelagic material. We use the age of turbidite B for the date of the El Golfo collapse in this study.

The Icod, Orotava, and Guimar landslides are the best-dated landslides from Tenerife. The Guimar landslide (120 km<sup>3</sup>) [Krstel *et al.*, 2001] correlates with turbidite Z in the Madeira Abyssal Basin [Hunt *et al.*, 2013], which places the events via biostratigraphic ages at  $850 \pm 10$  ka. The Orotava and Icod landslides, north of Tenerife, correlate with large amphitheatre-shaped depressions. The minimum age of the Orotava landslide is deduced from the oldest lava flow (PS4) infilling the Orotava Valley ( $534 \pm 9$  ka) [Boulestex *et al.*, 2013], and the maximum age from lavas intersected by the landslide scar ( $558 \pm 8$  ka). The landslide also correlates with turbidite MO in the Madeira Abyssal Plain, dated at  $540 \pm 5$  ka using biostratigraphy [Hunt *et al.*, 2013]. Subaerial dating suggests the Icod landslide occurred between  $175 \pm 3$  ka and  $161 \pm 5$  ka by K-Ar dating material that are incised by and infill the landslide scar, respectively [Boulestex *et al.*, 2011] but more recently Hunt *et al.*, [2013] used turbidite G in the Madeira Abyssal Plain to obtain a biostratigraphic age of  $165 \pm 5$  ka, which we use here.

Offshore La Palma, the Cumbre Nueva landslide is well dated. The headwall of the landslide has been identified as the prominent Cumbre Nueva Ridge that encloses a horseshoe-shaped depression [Urgeles *et al.*, 1999]. The Cumbre Nueva landslide is thought to have occurred after the emplacement of the Upper Taburiente volcanic deposits ( $566 \pm 8$  ka) and was followed by the emplacement of the Bejenado volcano ( $537 \pm 8$  ka) in the landslide scar [Guillou *et al.*, 1998, 2001; Carracedo *et al.*, 2001]. Hunt *et al.* [2013] date the Cumbre Nueva landslide at  $480 \pm 5$  ka by correlating the landslide with turbidite N in the Madeira

**Table 3.** Global Landslide Database for Ocean Island Landslides and Island Arc Landslides With Volumes >0.3 km<sup>3</sup> and With Age Errors of < ±22.5 kyr

Flank Collapse Name	Country/Island	Age (ka)	Volume (km <sup>3</sup> )	References	Letter in Supporting Information Figure S4
<b>Ocean Islands</b>					
El Golfo	Canary Islands, El Heirro	20–10	150	Weaver et al. [1992]; Longpre et al. [2011]; Hunt et al. [2013]	a
El Julan	Canary Islands, El Heirro	550–530	130	Hunt et al. [2013]	b
Cumbre Nueva	Canary Islands, La Palma	574–529	95	Costa et al. [2014]	c
Icod	Canary Islands, Tenerife	170–160	320	Ancochea et al. [1990]; Wynn et al. [2002]; Carracedo et al. [2007]; Hunt et al., [2013, 2014]	d
Orotava	Canary Islands, Tenerife	566–525	1000	Watts and Masson [1995]; Masson et al. [2002]; Boulestreix et al. [2013]; Hunt et al. [2013]	e
Guimar	Canary Islands, Tenerife	860–840	120	Krastel et al., [2001]	f
Fogo	Cape Verde	80–66	160	Ramalho et al., [2015]	g
Alika 2	Hawaii, Mauna Loa	132–122	>0.5	McMurty et al. [1999]	h
Tahiti North	Tahitian Archipelago, Tahiti	870–850	800	Clouard et al. [2000]; Hildenbrand et al. [2004, 2006]	i
<b>Island Arcs</b>					
Carmichaël	Lesser Antilles, Guadeloupe	11.5–6.9	0.3	Boudon et al. [1984, 2007]	j
Carbet	Lesser Antilles, Guadeloupe	3.5–2.8	0.5	Boudon et al., [1984, 2007]; Jerime [1979]; Paterne [1980]; Dagain [1981]; Dagain et al. [1981]	k
La Soufriere	Lesser Antilles, Dominica	6.7–2.3	6–7	Le Friant et al. [2002]; Boudon et al. [2007]	l
South	Italy, Ischia	3–2.4	1.5	De Alteriis et al. [2010, 2014]	m
Pietre Rosse	Italy, Ischia	40–2.4	>0.3	Vezzoli [1988]; Buchner [1986]; Seta et al. [2012]	n
Falanga	Italy, Ischia	2.4	>0.3	Buchner [1986]; Seta et al. [2012]	o
Casamicciola (NDDe)	Italy, Ischia	2.8	>0.3	de Vita et al. [2010]; Seta et al. [2012]	p
NDDw	Italy, Ischia	<10 ka		Vezzoli [1988]; de Aleriis and Violante [2009]; Seta et al. [2012]	q
D1	Lesser Antilles Martinique	129–124	>25	Germa et al. [2011]	r
D2 or the St Pierre event	Lesser Antilles, Martinique	23.6–26.4	13	Vincent et al. [1989]; Le Friant et al. [2003]	s
D3 or Rivière Sèche event	Lesser Antilles, Martinique	9.8–8	2	Le Friant et al. [2003]; Boudon et al. [2007]	t
Usu	Japan, Hokkaido	8–7	1–2	Moriya [2003] (in Japanese); Soya et al. [2007]; Yoshida et al. [2012]	u
Ritter	Papua New Guinea, Ritter Island	0.1	5	Cooke [1981]; Ward and Day [2003]	v
Deposit 1	Lesser Antilles, Montserrat	14–11	1.8	Trofimovs et al. [2013]; Watt et al. [2012a, 2012b]; Le Friant et al. [2004]; Lebas et al. [2011]	w
Deposit 2	Lesser Antilles, Montserrat	146–112	9	Harford et al. [2002]; Le Friant et al. [2004]; Lebas et al. [2011]; Watt et al. [2012a, 2012b]; Crutchley et al. [2013]	x
Deposit 5	Lesser Antilles, Montserrat	12–8	0.3	Cassidy et al. [2013]; Le Friant et al. [2004]; Lebas et al. [2011]	y

Abyssal Plain. This contrasts with subaerial dating, and we preferentially use the subaerial dates, because turbidite N may correlate with a younger landslide from La Palma.

To the east of Pico del Fogo in the Cape Verde Islands is a 130–160 km<sup>3</sup> landslide deposit [Lebas et al., 2007; Masson et al., 2008], which has been correlated with fields of boulders and chaotic conglomerates (interpreted as tsunami deposits) on the nearby island of Santiago [Ramalho et al., 2015]. <sup>3</sup>He dating of these tsunami deposits suggests a landslide age of 73 ± 7 ka [Ramalho et al., 2015]. This is close in age to a post collapse lava flow on Pico del Fogo dated at 86 ± 3 ka [Paris et al., 2011].

In the Hawaiian Archipelago at least 68 large volume landslides (up to 5000 km<sup>3</sup>) have been identified [Moore et al., 1989; Moore and Holcomb, 1994]. However, only the Alika 2 deposit, offshore Mauna Loa, is well dated. Cores F88 B-13, F91 39B1, and F91 4082 sample the Alika 2 deposit. Planktonic forams within the Alika 2 deposit date the landslide at 127 ± 5 ka using oxygen isotope stratigraphy [McMurty et al., 1999].

The island of Tahiti has two horseshoe-shaped depressions to the north and south of the island that correlate with large hummocky landslide deposits offshore with respective volumes of 800 and 1150 km<sup>3</sup> [Hildenbrand *et al.*, 2004]. The Tahitian shield was constructed between 1.4 and 8.7 Ma [Hildenbrand *et al.*, 2004], with vent locations concentrated along an E-W rift down the center of the island. Late activity along these vents (~870 ka) is thought to have triggered the two landslides [Hildenbrand *et al.*, 2004]. After the landslides, activity moved to the north, infilling the northern crater (851 ± 11 ka) [Hildenbrand *et al.*, 2004]. We therefore assume an age range for the northern landslide between 870 and 851 ± 11 ka. The southern crater is dated at ~500 ka, but is too poorly constrained to be included in the database.

#### 5.4.2. Island Arc Landslides

Evidence of large landslides has been identified at several islands in the Lesser Antilles (in addition to Montserrat). At Guadeloupe, subaerial exposures allow two events, the Carmichael and Carbet landslides, to be well dated [Boudon *et al.*, 1984, 1987, 2007]. The Carmichael landslide covers 17 km<sup>2</sup> onshore, and large blocky deposits are observed offshore [Boudon *et al.*, 1984]. The landslide is thought to be associated with the Carmichael crater that has a volume of 0.3 km<sup>3</sup>. Uncarbonized wood found within the deposit yields <sup>14</sup>C ages of 8400 ± 1500 to 11,270 ± 185 BP [Boudon *et al.*, 1984]. The Carbet landslide (estimated volume of 0.5 km<sup>3</sup>) is dated by subaerial outcrops along the Rivière du Carbet, where uncarbonized wood within the deposits yielded <sup>14</sup>C dates between 2800 and 3450 BP [Boudon *et al.*, 1984, 2007; Dagain *et al.*, 1981].

On Dominica four large landslides are observed, but only the Soufriere event is well dated. The Soufriere event (estimated volume 6–7 km<sup>3</sup>) formed from the collapse of the Plat Pays volcanic edifice [Le Friant *et al.*, 2002]. The lower bound age constraint is from <sup>14</sup>C dating of carbonaceous material found within a pyroclastic flow deposit from the Plat-Pays volcano dated at 6600 ± 50 ka. An upper bound comes from <sup>14</sup>C dating material (2380 ± 75 ka) from a tephra fall that overlies a mega block from the landslide (Scotts Head) [Le Friant *et al.*, 2002].

On Martinique, three of the four large landslide deposits are well dated (D1, D2, and D3). The D1 event is associated with a large west-facing landslide scar and has an estimated volume of 25 km<sup>3</sup>. The northern rim of the crater is well exposed, but the southern rim may have been destroyed and/or covered by later landslide events [Boudon *et al.*, 2007]. K-Ar dating of material infilling and incised by the landslide scar are dated at 126 ± 2 ka and 127 ± 2 ka, respectively. The D2, or St Pierre event formed a large west-facing amphitheatre-shaped structure and produced an offshore deposit with a volume of >13 km<sup>3</sup>. The upper bound date is given by U-Th disequilibrium dating of material intersected/outside the D2 structure, yielding ages of 37 ± 4 ka (Mont Calebasse lava dome) and 25 ± 1 ka (Mourne Plumé lava dome) [Le Friant *et al.*, 2003]. The lower bound age, of 25,000 ± 1040 years, is given by a <sup>14</sup>C charcoal age from a scoria flow deposit that in-fills the D2 structure [Vincent *et al.* 1989]. D3, or the Rivière Sèche event, has an estimated volume of 2 km<sup>3</sup>. The Aileron lava dome (summit part of Montagne Pelée) is intersected by the D3 structure and is dated at 9.7 ± 0.5 ka, providing an upper age limit [Le Friant *et al.*, 2003]. The “Sans Nom” lava dome in-fills the D3 structure and is dated at 9 ± 1 ka [Le Friant *et al.*, 2003].

Further afield, multiple large landslide deposits have been identified on and offshore Ischia, Italy [Chiocci and de Alteriis, 2006; De Alteriis and Violante, 2009], five of which are well dated. The South landslide (1.5 km<sup>3</sup>) is correlated with the offshore DF1 deposit and is dated at 2.4–3 ka (<sup>14</sup>C on planktonic forams within hemipelagic material above and below DF1) [De Alteriis *et al.*, 2010]. The Falanga and Pietre Rosse landslides outcrop to the east of Ischia, with a combined offshore volume of 11 km<sup>3</sup>. The Falanga deposit is dated at 400 BC based on historical chronicles [Buchner 1986]. The Pietre Rosse landslide has a maximum age constraint as it overlies the Citara Formation 40 ka [Vezzoli, 1988], and the upper bound age is given by the overlying Falanga landslide.

To the north of Ischia, two large landslide deposits (NDDe and NDDw) are seen [De Alteriis and Violante 2009]. The NDDe correlates onshore with the Casamicciola and Lacco Ameno landslide deposits [Seta *et al.*, 2012]. The Lacco Ameno deposit is poorly dated and is not included within the global database. The Casamicciola deposit overlies the Punta La Scrofa Tuff, dated at <800 BC [De Vita *et al.*, 2010]. Within seismic reflection profiles, a horizon beneath NDDw has been correlated with the onshore Zaro lava flow, dated at 6 ± 2 ka and 9 ± 1 ka using K-Ar dating [Vezzoli, 1988; de Aleriis and Violante, 2009]. Although the Casamicciola and NDDw have no upper bounds, the ages are within the error of ±22.5 kyr, and so are included within the global data set.

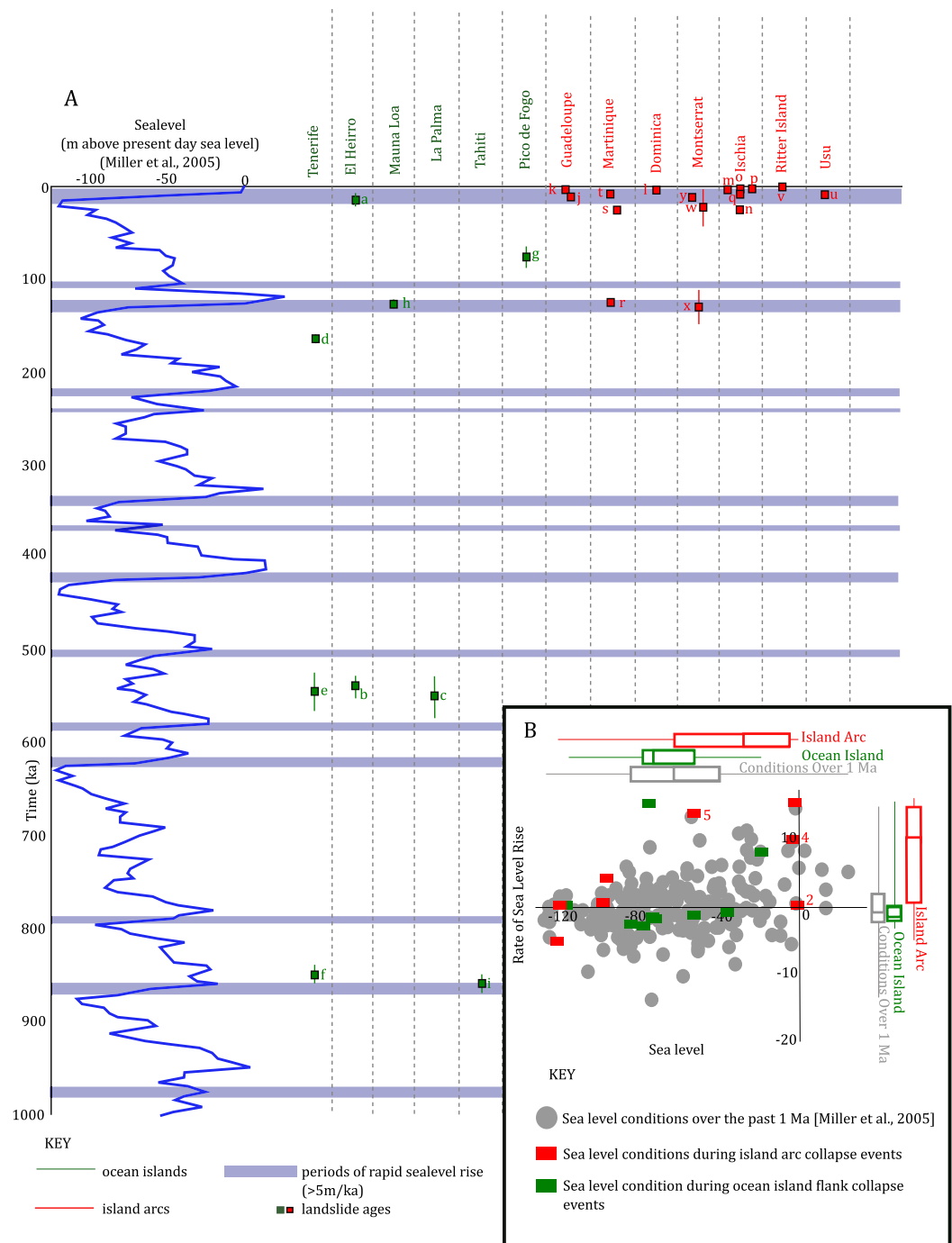


**Figure 6.** (a) Diagram summarizing the age of large (>0.3 km<sup>3</sup>) landslides around volcanic islands and sea level. The sea level curve used is Miller et al. [2005]. Events considered have date errors of <±22.5 ka. Periods of rapid sea level rise (>5m/ka) are highlighted in blue. Vertical bars show errors of individual landslide ages. Ocean island landslides are shown in green, and island arc landslides are shown in red. Letters identify individual landslides and correspond to letters in Table 3. (b) Comparison of sea level conditions with those at the time of documented landslides (Table 3) using data in 5 ka bins. Grey solid circles indicate the full range of conditions over the past 1 Ma at which no landslides were recorded. Annotated box and whisker plots indicate the spread of each data set, with boxes showing 25%, 50%, and 75% of the data, whiskers showing the minimum and maximum, and numbers next to data points show the number of overlapping datum. A general skew of landslides occurring at rapid sea level rises can be seen in the box and whisker plots.

The Japanese volcano of Usu is situated in the South of the Japanese island of Hokkaido. Usu formed ~20 ka [Soya et al., 2007] and after the edifice reached 1000 m, there was a large summit collapse (1–2 km<sup>3</sup>). This collapse, named the Zenkojii collapse, occurred at ~7–8 ka based on subaerial dating of infilling and cross-cut deposits [Moriya, 2003 (in Japanese); Soya et al., 2007].

A large 5 km<sup>3</sup> collapse from Ritter island (offshore New Guinea), which occurred 13 March 1888, is also included in the global database [Cooke 1981; Ward and Day 2003].

### 5.5. Large-Scale Flank Collapse and Sea Level: Comparison to Global Records

At Montserrat, the three well-dated large landslides from Soufrière Hills coincide with periods of rapid sea level rise. Using the global compilation, box and whisker plots (Figure 6) show that landslide occurrences at other island volcanoes are skewed towards periods of more rapid sea level rise. In contrast, at ocean islands the distribution of event timing shows no clear correlation with specific regimes of sea level (Figure 6). This is supported by preliminary statistical analyses (Mann-Whitney and Kolmogorov-Smirnov tests, see supporting information).

The global data set of landslide ages is restricted (9 events from ocean islands, 16 events from island arcs). Dating landslide deposits is challenging, because most material is emplaced offshore in poorly accessible, deep marine settings, typically comprising chaotic mixtures of material. Direct dating of material within landslides only provides maximum age constraints of landslide emplacement, unless material such as vegetation incorporated into the landslide deposits can be identified and dated. Indirect dating of material overlying and underlying landslide deposits or scars can result in large age gaps. Consequently the global landslide database is sparse, and dominated by a very few well-studied regions (e.g., Ischia, Lesser Antilles). Even in other regions where numerous events have been identified (e.g., Aleutian Islands) [Coombs *et al.*, 2007], very few events are dated, and so are excluded from our data set.

Given the limitations of a restricted data set, it is thus difficult to test the strength of the observed correlation between event timing and sea level change. Furthermore, the island arc database is biased toward recent landslide events (<20 ka), which includes a period of rapid sea level rise (Figure 6). Thus the apparent prevalence of island arc landslides during periods of rapid sea level rise could also be affected by a temporal record bias. Further investigation (by substantially increasing the dated landslide database) is required to test this initial result, which suggests a difference between how sea level change influences flank stability in island arc and ocean island settings.

Nevertheless, it is worth briefly considering the processes by which sea level rise may increase the likelihood of flank collapse at island-arc volcanoes. A ~100 m rise in sea level potentially enhances both dyke ascent (and hence volcanism) and fault movement in island-arc settings [cf., Nakada and Yokose, 1992], although the relationship between volcanism and sea level change may be complex [McGuire *et al.*, 1997] and is incompletely understood. Overpressure in magma chambers, which decreases by viscoelastic relaxation, is more sensitive to loading rate than the absolute load [Jellinek *et al.*, 2004] consistent with the observed correlation of collapse rapid sea level rise. Furthermore, sea level rise may result in greater magma-water interaction encouraging explosive, phreatomagmatic behavior. Such explosive behavior may reduce flank stability. An incipient instability within a volcanic edifice may also move closer to a critical failure point due either to direct stress increases associated with sea level rise, possibly combined with other factors. These may include enhanced erosion and modification of the groundwater system associated with rapid sea level change. Although the consequence of sea level rise on groundwater may depend on local factors, pore-pressure increases within hydrothermal systems have been suggested as a cause of edifice collapse [Elsworth and Voight, 1995; Day, 1996; Reid, 2004].

Our results suggest that these factors may be less significant in ocean-island settings, but the reason for this is as yet unclear. Structurally, the more basaltic composition of ocean islands means they are likely to have more stable flanks than island arcs, with a broader profile and lower slope gradients [Watt *et al.*, 2014], yet the presence of widespread landslide deposits around many ocean islands indicates that they are still prone to catastrophic flank failure.

## 6. Conclusions

In contrast to the subaerial stratigraphic record, volcanoclastic layers within IODP Hole U1395B provide a more complete record of volcanism on Montserrat. Periods of reduced event frequency (interpreted as periods of volcanic quiescence) last of the order 10<sup>4</sup>–10<sup>5</sup> ka, substantially less than apparent gaps in the subaerial record. The pauses in activity suggested by the subaerial record are likely to be a manifestation of poor preservation and burial of onshore stratigraphy, coupled with the predominantly offshore deposition of

volcanic products. The marine record reveals that three periods of heightened volcanic activity at Montserrat occurred at ~930 to ~900 ka, ~810 to ~760 ka (both during the Centre Hills period), and ~190 to ~120 ka (during the Soufrière Hills period). A notable increase in event frequency at ~810 to ~760 ka coincides with the occurrence of mafic scoria in Hole U1395B, while the peak in Soufrière Hills volcanism coincides with the largest flank collapse from the volcano (130 ka) and a brief switch to mafic volcanism.

Periods of heightened volcanic activity coincide with periods of increased turbidite occurrence, suggesting that intensified volcanic activity may facilitate mass-wasting processes. No statistically significant correlation of turbidite occurrence (collapse frequency) and sea level were observed, but all of the well-dated and large-scale landslides on Montserrat occurred during periods of rapid sea level rise. While the global data set is small and there are uncertainties associated with dating landslide events, this pattern of large-scale landslides coinciding with periods of rapid sea level rise is replicated within a global data set for island-arc volcanoes, but not at ocean islands. The reasons for this difference between island arcs and ocean islands remain unclear, but may reflect a greater susceptibility of the steeper, more lithologically diverse flanks of island-arc volcanoes to rapid sea level changes, relative to ocean islands.

### Acknowledgments

We would like to thank all of the members on the Expedition 340 science party for their hard work during and after the cruise. We would also like to thank the captain of the RN *JOIDES Resolution* and the crew, staff, and the shipboard scientists of Expedition 340 for their work during the cruise. Many thanks to the staff at Texas Agricultural and Mechanical University who sampled Hole U1395B. Mike Cassidy acknowledges a *Alexander Von Humboldt* grant. S.W. acknowledges NERC grants NE/K000403/1 and NE/102044X/1. Radiocarbon dates were funded by NERC under allocation SUERC 1721.0513 at the NERC radiocarbon facility. Thanks to Suzanne MacLachlan in BOSCORF for providing lab space and equipment. Finally thanks to the two anonymous reviewers for their insightful feedback. Supporting data has been included in four supporting information tables, a supporting information file, and a supporting information figure file. Any further data can be obtained from Maya Coussens (mfc1e12@soton.ac.uk or maya.pratt@mail.com) and IODP LIMS reports (<http://web.iodp.tamu.edu/UWQ/>).

### References

- Ablay, G. J., and J. Marti (2000), Stratigraphy, structure, and volcanic evolution of the Pico Teide-Pico Viejo formation, Tenerife, Canary Islands, *J. Volcanol. Geotherm. Res.*, *103*, 175–208.
- Ancochea, E., J. M. Fuster, E. Ibarrola, A. Cendrero, J. Coello, F. Hernan, J. M. Cantagrel, and C. Jamond (1990), Evolution of the island of Tenerife (Canary Islands) in the light of new K-Ar data, *J. Volcanol. Geotherm. Res.*, *44*, 231–249.
- Boudon, G., M. P. Semet, and P. M. Vincent (1984), Flank failure-directed blast eruption at Soufrière, Guadeloupe, French West Indies: A 3,000-yr-old Mt. St. Helens?, *Geology*, *12*(6), 350–353.
- Boudon, G., M. P. Semet, and P. M. Vincent (1987), Magma and hydrothermally driven sector collapses: The 3100 and 11,500 y. BP eruptions of la Grande Découverte (la Soufrière) volcano, Guadeloupe, French West Indies, *J. Volcanol. Geotherm. Res.*, *33*(4), 317–323.
- Boudon, G., A. Le Friant, J. C. Komorowski, C. Deplus and M. P. Semet (2007), Volcano flank instability in the Lesser Antilles Arc: Diversity of scale, processes, and temporal recurrence, *J. Geophys. Res.*, *112*, B08205, doi:10.1029/2006JB004674.
- Boulestix, T., A. Hildenbrand, V. Soler, X. Quidelleur, and P. Y. Gillot (2013), Coeval giant landslides in the Canary Islands: implications for global, regional and local triggers of giant flank collapses on oceanic volcanoes, *J. Volcanol. Geotherm. Res.*, *257*, 90–98.
- Boulestix, T., A. Hildenbrand, P.-Y. Gillot and V. Soler (2011), Eruptive response of oceanic islands to giant landslides: New insights from the geomorphologic evolution of the Teide–Pico Viejo volcanic complex (Tenerife, Canary), *Geomorphology*, *138*, 61–73.
- Buchner, G. (1986), Eruzioni vulcaniche e fenomeni vulcano-tettonici di età preistorica e storica nell' isola di Ischia, in *Tremblements de terre, éruptions volcaniques et vie des hommes dans la Campanie antique*, Vol. 7, edited by C. Albore-Livadie, pp. 145–188, Cent. Jean Bérard, Napoli.
- Cande, S. C., and D. V. Kent (1992a), A new geomagnetic polarity time scale for the Late Cretaceous and Cenozoic, *J. Geophys. Res.*, *97*, 13,917–13,951.
- Cande, S. C., and D. V. Kent (1992b), Ultrahigh resolution of marine magnetic anomaly profiles: A record of continuous paleointensity variations?, *J. Geophys. Res.*, *97*, 15,075–15,083.
- Cande, S. C., and D. V. Kent (1995), Revised calibration of the geomagnetic polarity timescale for the Late Cretaceous and Cenozoic, *J. Geophys. Res.*, *100*, 6093–6095.
- Carracedo, J. C., E. Rodríguez Badiola, H. Guillou, J. De La Nuez, and F. J. Pérez Torrado (2001), Geology and volcanology of La Palma and El Hierro (Canary Islands), *Estudios Geológicos*, *57*, 175–273. [Available at <http://hdl.handle.net/10261/2343>.]
- Carracedo, J. C., E. Rodríguez Badiola, H. Guillou, M. Paterne, S. Scaillet, F. J. Pérez Torrado, R. Paris, U. Fra-Paleo, and A. Hansen (2007), Eruptive and structural history of Teide Volcano and rift zones of Tenerife, Canary Islands, *Geol. Soc. Amer. Bull.*, *119*, 9–10, 1027–1051, doi: 10.1130/b26087.1.
- Cassidy, M., R. N. Taylor, M. R. Palmer, R. Cooper, C. Stenlake, and J. Trofimovs (2012a) Tracking the magmatic evolution of an island arc volcano: Insights from a high-precision Pb isotope record of Montserrat, Lesser Antilles, *Geochem. Geophys. Geosyst.*, *13*, Q05003, doi: 10.1029/2012GC004064.
- Cassidy, M., J. Trofimovs, S. F. L. Watt, M. R. Palmer, R. N. Taylor, T. M. Gernon, P. J. Talling, and A. Le Friant (2012b), Multi-stage collapse events in the South Soufrière Hills, Montserrat, as recorded in marine sediment cores, in *In the Eruption of Soufrière Hills Volcano, Montserrat From 2000-2010*, edited by G. Wadge et al., *Geol. Soc. Spec. Publ.*, *39*, 383–397.
- Cassidy, M., J. Trofimovs, M. R. Palmer, P. J. Talling, S. F. L. Watt, S. G. Moreton, and R. N. Taylor (2013), Timing and emplacement dynamics of newly recognised mass flow deposits at ~8-12 ka offshore Soufrière Hills volcano, Montserrat: How submarine stratigraphy can complement subaerial eruption histories, *J. Volcanol. Geotherm. Res.*, *253*, 1–14, doi:10.1016/j.jvolgeos.2012.12.002.
- Cassidy, M., S. F. L. Watt, M. R. Palmer, J. Trofimovs, W. Symons, S. E. Maclachlan and A. J. Stinton (2014), Construction of volcanic records from marine sediment cores: A review and case study (Montserrat, West Indies), *Earth Sci. Rev.*, *138*, 137–155, doi:10.1016/j.earscirev.2014.08.008.
- Cassidy, M., et al. (2015), Rapid onset of mafic magmatism facilitated by volcanic edifice collapse, *Geophys. Res. Lett.*, *42*, 4778–4785, doi: 10.1002/2015GL064519.
- Chiocci, F. L., and G. De Alteriis (2006), The Ischia debris avalanche: first clear submarine evidence in the Mediterranean of a volcanic island prehistorical collapse, *Terra Nova*, *18*(3), 202–209, doi:10.1111/j.1365-3121.2006.00680.x.
- Clare, M. A., P. J. Talling, P. H. Challenor, and J. E. Hunt (2016), Tempo and triggering of large submarine landslides: Statistical analysis for hazard assessment, in *Submarine Mass Movements and Their Consequences*, vol. 41, edited by G. Lamarche et al., pp. 509–517, Springer, Dordrecht, Netherlands.
- Clouard, V., A. Bonneville, and G. Pierre-Yves (2001), A giant landslide on the southern flank of Tahiti Island, French Polynesia, *Geophys. Res. Lett.*, *28*, 11, 2253–2256.

- Cole, P. D., E. S. Calder, R. S. J. Sparks, A. B. Clarke, T. H. Druitt, S. R. Young, and G. E. Norton (2002), Deposits from dome-collapse and fountain-collapse pyroclastic flows at Soufrière Hills Volcano, Montserrat, *Geol. Soc. London Mem.*, 21(1), 231–262.
- Collins, B. D., and T. Dunne (1986), Erosion of tephra from the 1980 eruption of Mount St. Helens, *Geol. Soc. Am. Bull.*, 97(7), 896–905.
- Cooke, R. J. S. (1981), Eruptive history of the volcano at Ritter Is-land, in *Cooke–Ravian Volume of Volcanological Papers, In Geological Survey of Papua New Guinea Memoir*, vol. 10, edited by R. W. Johnson, pp. 115–123, Office of Minerals and Energy, Port Moresby, Papua New Guinea.
- Coombs, M. L., S. M. White, and D. W. Scholl (2007), Massive edifice failure at Aleutian arc volcanoes, *Earth Planet. Sci. Lett.*, 256(3), 403–418.
- Costa, A. C. G., F. O. Marques, A. Hildenbrand, A. L. R. Sibrant, and C. M. S. Catita (2014), Large-scale catastrophic flank collapses in a steep volcanic ridge: the Pico-Faial Ridge, Azores Triple Junction, *J. Volcanol. Geotherm. Res.*, 272, 111–125, doi:10.1016/j.jvolgeores.2014.01.002.
- Coussens M, et al. (2016), Synthesis: Stratigraphy and age control for IODP Sites U1394, U1395, and U1396 offshore Montserrat in the Lesser Antilles, in *Proceedings of the Integrated Ocean Drilling Program*, principal investigators A. Le Friant, O. Ishizuka, and N. A. Stronck, vol. 340, Ocean Drill. Program, College Station, Tex.
- Crutchley, G. J., et al. (2013), Insights into the emplacement dynamics of volcanic landslides from high-resolution 3D seismic data acquired offshore Montserrat, Lesser Antillies, *Mar. Geol.*, 335, 1–15, doi:10.1016/j.margeo.2012.10.004.
- Dagain, J. (1981), La mise en place du massif volcanique Madaleine—Soufrière, Basse-Terre de Guadeloupe, Antilles, 3rd cycle thesis, Univ. Paris Sud, Orsay, France.
- Dagain, J., M. Paterne, and D. Westercamp (1981), La mise en place du massif Madeleine-Soufrière, Basse-Terre de Guadeloupe, Antilles, C. R. Acad. Sci., 11(292), 921–926.
- Day, S. J. (1996), Hydrothermal pore fluid pressure and the stability of porous, permeable volcanoes, in *Volcano Instability on the Earth and Other Planets*, edited by W. J. McGuire and A. P. Jones, *Geol. Soc. Spec. Publ.*, 110, 77–93.
- De Alteriis, G., and C. Violante (2009), Catastrophic landslides off Ischia volcanic island (Italy) during prehistory, *Geol. Soc. Spec. Publ.*, 322(1), 73–104.
- De Alteriis, G., D. D. Insinga, S. Morabito, V. Morra, F. L. Chiocci, F. Terrasi, C. Lubritto, C. Di Benedetto, and M. Pazzaneses (2010), Age of submarine debris avalanches and tephrostratigraphy offshore Ischia Island, Tyrrhenian Sea, Italy, *Mar. Geol.*, 278, 1–18, doi:10.1016/j.margeo.2010.08.004.
- De Alteriis, G., A. S. di Scotto, F. L. Chiocci, M. Ramondini, and C. Violante (2014), The Case of Ischia Underwater Debris Avalanche (Italy, Tyrrhenian Sea) and Its High Mobility, In *Engineering Geology for Society and Territory-Volume 4*, edited by G. Lollino, et al., pp. 227–232, Springer, Dordrecht, Netherlands.
- Deplus, C., A. Le Friant, G. Boudon, J. C. Komorowski, B. Vilement, C. Harford, J. Segoufin, and J. L. Chiminee (2001), Submarine evidence for large-scale debris avalanches in the Lesser Antillies Arc, *Earth Planet. Sci. Lett.*, 192, 145–157.
- De Vita, S., F. Sansivero, G. Orsi, E. Marotta, and M. Piochi (2010), Volcanological and structural evolution of the Ischia resurgent caldera (Italy) over the past 10 ky. *Geol. Soc. Am. Spec. Pap.*, 464, 193–239.
- Elsworth, D., and B. Voight (1995), Dike intrusion as a trigger for large earthquakes and the failure of volcano flanks, *J. Geophys. Res.*, 100, 6005–6024.
- Folk, R. L., and W. C. Ward (1957), Brazos River bar: A study in the significance of grain size parameters, *J. Sediment. Petrol.*, 27, 3–26.
- Gee, M. J. R., D. G. Masson, A. B. Watts, and P. A. Allen (2001a), The Saharan Debris Flow: An insight into the mechanics of long runout debris flows, *Sedimentology*, 46, 317–335.
- Gee, M. J. R., A. B. Watts, D. G. Masson and N. C. Mitchell (2001b), Landslides and the evolution of El Hierro in the Canary Islands, *Mar. Geol.*, 177, 271–293.
- Germa, A., X. Quidelleur, S. Labanieh, P. Lahitte, and C. Chauvel (2010), The eruptive history of Morne Jacob volcano (Martinique Island, French West Indies): Geochronology, geomorphology and geochemistry of the earliest volcanism in the recent Lesser Antilles arc, *J. Volcanol. Geotherm. Res.*, 198(3–4), 297–310, doi:10.1016/j.jvolgeores.2010.09.013.
- Germa, A., X. Quidelleur, P. Lahitte, S. Labanieh, and C. Chauvel (2011), The K-Ar Cassagnol-Gillot technique applied to wester Martinique lavas: A record of Lesser Antilles arc activity from 2 Ma to Mount Pelee volcanism, *Quat. Geol.*, 6, 341–355.
- Guillou, H., J. C. Carracedo, F. P. Torrado, and E. R. Badiola (1996), K-Ar ages and magnetic stratigraphy of a hotspot-induced, fast grown oceanic island: El Hierro, Canary Islands, *J. Volcanol. Geotherm. Res.*, 73(1), 141–155.
- Guillou, H., J. C. Carracedo, and S. J. Day (1998), Dating of the upper Pleistocene–Holocene volcanic activity of La Palma using the unspiked K-Ar technique, *J. Volcanol. Geotherm. Res.*, 86(1), 137–149.
- Guillou, H., J. C. Carracedo, and R. A. Duncan (2001), K-Ar, 40 Ar–39 Ar ages and magnetostratigraphy of Brunhes and Matuyama lava sequences from La Palma Island, *J. Volcanol. Geotherm. Res.*, 106(3), 175–194.
- Hatfield, R., and Expedition 340 Scientists (2013), Paleomagnetism in methods, in *Proceedings of IODP, 340: Tokyo (Integrated Ocean Drilling Program Management International, Inc.)*, edited by A. Le Friant et al., doi:10.2204/iodp.proc.340.102.2013.
- Harford, C. L., M. S. Pringle, R. S. J. Sparks, and S. R. Young (2002), The volcanic evolution of Montserrat using 40Ar/39Ar geochronology, *Geol. Soc. London Mem.*, 21, 93–113, doi:10.1144/GSL.MEM.2002.021.01.05.
- Herd, R. A., M. Edmonds, and V. Bass (2006), Catastrophic lava dome failure at Soufriere Hills Volcano, Montserrat 12–13 July 2003, *J. Volcanol. Geotherm. Res.*, 148, 234–252.
- Hildenbrand, A., P.-Y. Gillot, and I. Le Roy (2004), Volcano-tectonic and geochemical evolution of an oceanic intra-plate volcano: Tahiti-Nui (French Polynesia), *Earth Planet. Sci. Lett.*, 217, 349–365.
- Hildenbrand, A., P. Y. Gillot, and A. Bonneville (2006), Offshore evidence for a huge landslide of the northern flank of Tahiti-Nui (French Polynesia), *Geochem. Geophys. Geosys.*, 7(3), doi:10.1029/2005GC001003.
- Houghton, B. F., C. J. N. Wilson, M. O. McWilliams, M. A. Lanphere, S. D. Weaver, R. M. Briggs, and M. S. Pringle (1995), Volcanic Zone, New Zealand Chronology and dynamics of a large silicic magmatic system: Central Taupo Volcanic Zone, New Zealand, *Geology*, 23, 13–16, doi:10.1130/00917613(1995)023 <0013:CADOAL>2.3.CO;2.
- Hunt, J. E., R. B. Wynn, P. J. Talling, and D. G. Masson (2013), Turbidite record of frequency and source of large volume (>100 km<sup>3</sup>) Canary Island landslides in the last 1.5 Ma: Implications for landslide triggers and geohazards, *Geochem. Geophys. Geosyst.*, 14, 2100–2123, doi:10.1002/ggge.20139.
- Hunt, J. E., P. J. Talling, M. Clare, I. Jarvis, and R. B. Wynn (2014), Long-term (17 Ma) turbidite record of the timing and frequency of large flank collapses of the Canary Islands, *Geochem. Geophys. Geosyst.*, 15, 3322–3345, doi:10.1002/2014GC005232.
- Jellinek, A. M., M. Manga, and M. O. Saar (2004) Did melting glaciers cause volcanic eruptions in eastern California? Probing the mechanics of dike formation, *J. Geophys. Res.*, 109, B09206, doi:10.1029/2004JB002978.
- Jérémie, J. J. (1979), Données préliminaires sur l'âge des importants lahars situés au sud ouest du massif de la Soufrière: Académie des Sciences, *Comptes Rendus, D-288*, 935–938.

- Jutzeler, M., J. D. L. White, P. J. Talling, M. McCanta, S. Morgan, A. Le Friant and O. Ishizuka (2014), Coring disturbances in IODP piston cores with implication for offshore record of volcanic events and the Missoula megafloods *Geochem. Geophys. Geosyst.*, *15*, 3572–3590, doi:10.1002/2014GC005447.
- Kameo, K., and T. J. Bralower (1998), Neogene calcareous nannofossil biostratigraphy of sites 998, 999, and 1000, Caribbean Sea, *Proc. Ocean Drill. Program Sci. Results*, *165*, 3–17.
- Kokelaar, B. P. (2002), Setting, chronology and consequences of the eruption of Soufrière Hills Volcano, Montserrat (1995–1999), in *The Eruption of Soufrière Hills volcano, Montserrat, From 1995 to 1991*, edited by T. Druitt, and P. Kokelaar, *Geol. Soc. Spec. Publ.*, *21*, 1–43, doi:10.1144/GSL.MEM.2002.021.01.02.
- Krastel, S., H. U. Schmincke, C. L. Jacobs, R. Rihm, T. P. Le Bas, and B. Alibés (2001), Submarine landslides around the Canary Islands, *J. Geophys. Res.*, *106*, 3977–3997.
- Le Bas, T. P., D. G. Masson, R. Holtom, and I. Grevemeyer (2007), *Slope failures of the flanks of the southern Cape Verde Islands*, in *Submarine Mass Movements and their Consequences, Adv. in Nat. and Technol. Hazard Res.*, vol. 27, edited by V. Lykousis, D. Sakellariou, and J. Locat, pp. 337–346, Springer, Dordrecht, Netherlands.
- Lebas, E., S. F. L. Watt, P. J. Talling, N. Feuillet, C. Deplus, C. Berndt, and M. Vardy (2011), Multiple widespread landslides during the long-term evolution of a volcanic island: Insights from high-resolution seismic data, Montserrat, Lesser Antilles, *Geochem. Geophys. Geosyst.*, *12*, Q05006, doi:10.1029/2010GC003451.
- Le Friant, A., G. Boudon, J.-C. Komorowski, and C. Deplus (2002), L'île de la Dominique, à l'origine des avalanches de débris les plus volumineuses de l'arc des Petites Antilles, *C. R. Geosci.*, *334*, 235–243.
- Le Friant, A., G. Boudon, C. Deplus, and B. Villemont (2003), Large-scale flank collapse events during the activity of Montagne Pelée, Martinique, Lesser Antilles, *J. Geophys. Res.*, *108*(B1), 2055, doi:10.1029/2001JB001624.
- Le Friant, A., C. L. Harford, C. Deplus, G. Boudon, R. S. J. Sparks, R. A. Herd, and J. C. Komorowski (2004), Geomorphological evolution of Montserrat (West Indies): importance of flank collapse and erosional processes, *J. Geol. Soc.*, *161*(1), 147–160, doi:10.1144/0016-764903-017.
- Le Friant, A., E. J. Lock, M. B. Hart, G. Boudon, R. S. J. Sparks, M. J. Leng, C. W. Smart, J. C. Komorowski, C. Deplus, and J. K. Fisher (2008), Late Pleistocene tephrochronology of marine sediments adjacent to Montserrat, Lesser Antilles volcanic arc, *J. Geol. Soc.*, *165*(1), 279–289, doi:10.1144/0016-76492007-019.
- Le Friant, A., C. Deplus, and G. Boudon (2009), Submarine deposition of volcanoclastic material from the 1995–2005 eruptions of Soufrière Hills volcano, Montserrat, *J. Geol. Soc.*, *166*, 171–182, doi:10.1144/0016-76492008-047.
- Le Friant, A., et al. (2010), Eruption of Soufrière Hills (1995–2009) from an offshore perspective: Insights from repeated swath bathymetry surveys, *Geophys. Res. Lett.*, *37*, L11307, doi:10.1029/2010GL043580.
- Le Friant, A., et al. (2015), Submarine record of volcanic island construction and collapse in the Lesser Antilles arc: First scientific drilling of submarine volcanic island landslides by IODP Expedition 340, *Geochem. Geophys. Geosyst.*, *16*, 420–442, doi:10.1002/2014GC005652.
- Lisiecki, L. E., and M. E. Raymo (2005), A Pliocene-Pleistocene stack of 57 globally distributed benthic  $\delta^{18}\text{O}$  records, *Paleoceanography*, *20*, 1–17, doi:10.1029/2004PA001071.
- Longpré, M. A., J. P. Chadwick, J. Wijbrans, and R. Iping (2011), Age of the El Golfo debris avalanche, El Hierro (Canary Islands): New constraints from laser and furnace  $^{40}\text{Ar}/^{39}\text{Ar}$  dating, *J. Volcanol. Geotherm. Res.*, *203*, 76–80, doi:10.1016/j.jvolgeores.2011.04.002.
- Major, J. J., T. C. Pierson, R. L. Dinehart, and J. E. Costa (2000), Sediment yield following severe volcanic disturbance: A two-decade perspective from Mount St. Helens, *Geology*, *28*(9), 819–822.
- Marques, R., J. Zêzere, R. Trigo, J. Gaspar, and I. Trigo (2008), Rainfall patterns and critical values associated with landslides in Povoação County (São Miguel Island, Azores): Relationships with the North Atlantic Oscillation, *Hydrol. Processes*, *22*(4), 478–494.
- Masson, D. G. (1996), Catastrophic collapse of the volcanic island of Hierro 15 ka ago and the history of landslides in the Canary islands, *Geology*, *24*(3), 231–234.
- Masson, D. G., A. B. Watts, M. J. R. Gee, R. Urgeles, N. C. Mitchell, T. P. Le Bas, and M. Canals (2002), Slope failures on the flanks of the western Canary Islands, *Earth Sci. Rev.*, *57*, 1–35, doi:10.1016/S0012-8252(01)00069-1.
- Masson, D. G., C. B. Harbitz, R. B. Wynn, G. Pedersen, and F. Lovholt (2006), Submarine landslides: Processes, triggers and hazard prediction, *Philos. Trans. R. Soc.*, *364*, 2009–2039, doi:10.1098/rsta.2006.1810.
- Masson, D. G., T. P. Le Bas, I. Grevemeyer, and W. Weinrebe (2008), Flank collapse and large-scale landsliding in the Cape Verde Islands, off West Africa, *Geochem. Geophys. Geosyst.*, *9*, Q07015, doi:10.1029/2008GC001983.
- McGuire, W. J., R. J. Howarth, C. R. Firth, A. R. Solow, A. D. Pullen, S. J. Saunders, I. S. Stewart, and C. Vita-Finzi (1997), Correlation between rate of sea-level change and frequency of explosive volcanism in the Mediterranean, *Nature*, *389*, 473–477.
- McMurty, G. M., E. Herrero-Bervera, M. D. Cremer, J. R. Smith, J. Resig, C. Sherman, and M. E. Torresan (1999), Stratigraphic constraints on the timing and emplacement of the Alika 2 giant Hawaiian submarine landslide, *J. Volcanol. Geotherm. Res.*, *94*, 35–58.
- McMurty, G. M., P. Watts, G. J. Fryer, J. R. Smith, and F. Imamura (2004a), Giant landslides, mega-tsunamis, and paleo-sea level in the Hawaiian Islands, *Mar. Geol.*, *i*, 219–233, doi:10.1016/S0025-3227(03)00306-2.
- McMurty, G. M., G. J. Fryer, D. R. Tappin, I. P. Wilkinson, M. Williams, J. Fietzke, D. Garbe-Schoenberg, and P. Watts (2004b), Megatsunami deposits on Kohala volcano, Hawaii, from flank collapse of Mauna Loa, *Geology*, *32*(9), 741–744, doi:10.1130/G20642.1.
- Miller, K. G., M. A. Komins, J. V. Browning, J. D. Wright, G. S. Mountain, M. E. Katz, P. J. Sugarman, B. S. Cramer, N. Christie-Blick, and S. F. Pekar (2005), The Phanerozoic Record of Global Sea-Level Change, *Science*, *310*, 1293–1298, doi:10.1126/science.1116412.
- Moore, J. G., and R. T. Holcomb (1994), Giant Hawaiian landslides, *Earth Planet. Sci. Lett.*, *22*, 119–144.
- Moore, J. G., D. A. Clague, R. T. Holcomb, P. W. Lipman, W. R. Normark, and M. E. Torresan (1989), Prodigious submarine landslides on the Hawaiian Ridge, *J. Geophys. Res.*, *94*, 17,465–17,484.
- Moore, J. G., D. A. Clague, R. T. Holcomb, P. W. Lipman, W. R. Normark, and M. E. Torresan (1992), Prodigious submarine landslides on the Hawaiian Ridge, *J. Geophys. Res.*, *94*, 17,465–17,484.
- Moriya, I. (2003), Toya Caldera, in *Regional Geomorphology of the Japanese Islands*, vol. 2, pp. 281–288, edited by T. Koaze et al., Univ. of Tokyo Press, Tokyo, Japan.
- Nakada, M. and H. Yokose (1992), Ice age as a trigger of active quaternary volcanism and tectonism, *Tectonophysics*, *212*, 321–329.
- Ogg, J. G. (2012), Geomagnetic polarity time scale, in *The Geologic Time Scale 2012*, edited by F. M. Gradstein et al., pp. 85–114, Elsevier, Oxford, U. K.
- Palmer, M. R., et al. (2016), Discovery of a large 2.4 Ma Plinian eruption of Basse-Terre, Guadeloupe, from the marine sediment record, *Geology*, *44*(2), 123–126.
- Paris, R., T. Giachetti, J. Chevalier, H. Guillou, and N. Frank (2011), Tsunami deposits in Santiago Island (Cape Verde archipelago) as possible evidence of a massive flank failure of Fogos volcano, *Sediment. Geol.*, *239*(3), 129–145.

- Patene, M. (1980), Chronologie des éruptions récentes du massif de la Soufrière (Guadeloupe—Petites Antilles), Essai de comparaison des périodes d'activité volcanique de quelques grandes régions volcaniques, 3rd cycle thesis, no. 1606, 165 pp., Univ. de Bordeaux, Bordeaux, France.
- Pope, E. L., P. J. Talling, M. Urlaub, J. E. Hunt, M. A. Clare, and P. Challenor, (2015), Are large submarine landslides temporally random or do uncertainties in available age constraints make it impossible to tell?, *Mar. Geol.*, *369*, 19–33.
- Quidelleur, X., A. Hildenbrand, and A. Samper (2008), Causal link between Quaternary paleoclimatic changes and volcanic islands evolution, *Geophys. Res. Lett.*, *35*, L02303, doi:10.1029/2007GL031849.
- Radiosonde data (2012), From directory data-por/, Download file for Le Reuzet station in Guadeloupe, code GP, numeric code 78897, Asheville, USA. [Available at <http://www1.ncdc.noaa.gov/pub/data/igra/>]
- Ramalho, R. S., G. Winckler, J. Madeira, G. R. Helffrich, A. Hipólito, R. Quartau, and J. M. Schaefer (2015), Hazard potential of volcanic flank collapses raised by new megatsunami evidence, *Sci. Adv.*, *1*(9), e1500456.
- Reid, M. E. (2004), Massive collapse of volcano edifices triggered by hydrothermal pressurization, *Geology*, *32*, 373–376.
- Reid, R. P., S. N. Carey, and D. R. Ross (1996), Geological Society of America Bulletin Late Quaternary sedimentation in the Lesser Antilles island arc Late Quaternary sedimentation in the Lesser Antilles island arc, *Geol. Soc. Am. Bull.*, *108*, 78–100, doi:10.1130/0016-7606(1996)108<0078:LQSTIL>2.3.CO;2.
- Samper, A., X. Quidelleur, P. Lahitte, and D. Mollex (2007), Timing of effusive volcanism and collapse events within an oceanic arc island: Basse-Terre, Guadeloupe archipelago (Lesser Antilles Arc), *Earth Planet. Sci. Lett.*, *258*, 175–191, doi:10.1016/j.epsl.2007.03.030.
- Sato, H. P., H. Hasegawa., S. Fujiwara., M. Tobita., M. Koarai., H. Une, and J. Iwahashi (2007), Interpretation of landslide distribution triggered by the 2005 Northern Pakistan earthquake using SPOT 5 imagery, *Landslides*, *4*(2), 113–122.
- Seta, M. D., et al. (2012), Slope instability induced by volcano-tectonics as an additional source of hazard in active volcanic areas: The case of Ischia island (Italy), *Bull. Volcanol.*, *74*, 79–106.
- Siebert, L. (1984), Large volcanic debris avalanches: Characteristics of source areas, deposits, and associated eruptions, *J. Volcanol. Geotherm. Res.*, *22*, 163–197.
- Singer, B. S., B. R. Jicha, M. A. Harper, J. A. Naranjo, L. E. Lara, and H. Moreno-Roa (2008), Eruptive history, geochronology, and magmatic evolution of the Puyehue-Cordón Caulle volcanic complex, Chile, *Geol. Soc. Am. Bull.*, *120*(5/6), 599–618, doi:10.1130/B26276.1.
- Soya, T., Y. Katsui, K. Niida, K. Sakai and A. Tomiya (2007), *Geologic Map of Usu Volcano*, 2nd ed., Geological Map of Volcanoes (2), Geological Survey of Japan, The Natl. Inst. of Adv. Ind. Sci. and Technol., Tsukuba.
- Stillman, C. J. (1999), Giant Miocene landslides and the evolution of Fuerteventura, Canary Islands, *J. Volcanol. Geotherm. Res.*, *94*(1–4), 89–104.
- Trofimovs, J., et al. (2006), Submarine pyroclastic deposits formed at the Soufrière Hills volcano, Montserrat (1995–2003): What happens when pyroclastic flows enter the ocean? *Geology*, *34*(7), 549–552, doi:10.1130/G22424.1.
- Trofimovs, J., R. S. J. Sparks, and P. J. Talling (2008), Anatomy of a submarine pyroclastic flow and associated turbidity current: July 2003 dome collapse, Soufrière Hills volcano, Montserrat, West Indies, *Sedimentology*, *55*, 617–634, doi:10.1111/j.1365-3091.2007.00914.
- Trofimovs, J., et al. (2010), Evidence for carbonate platform failure during rapid sea-level rise; ca 14 000 year old bioclastic flow deposits in the Lesser Antilles, *Sedimentology*, *57*, 735–759, doi:10.1111/j.1365-3091.2009.01117.
- Trofimovs, J., et al. (2012), Submarine pyroclastic deposits formed during the 20th May 2006 dome collapse of Soufrière Hills volcano, Montserrat, *Bull. Volcanol.*, *74*, 391–405, doi:10.1007/s00445-011-0533-5.
- Trofimovs, J., et al. (2013), Timing, origin and emplacement dynamics of mass flows offshore of SE Montserrat in the last 110 ka: Implications for landslide and tsunami hazards, eruption history, and volcanic island evolution, *Geochem. Geophys. Geosyst.*, *14*, 385–406, doi:10.1002/ggge.20052.
- Urgeles, R., M. Canals, J. Baraza, and B. Alonso (1997), The most recent megalandslides of the Canary Islands: El Golfo debris avalanche and Canary debris flow, west El Hierro Island, *J. Geophys. Res.*, *102*, 20,305–20,323.
- Urgeles, R., D. G. Masson, M. Canals, A. B. Watts, and T. Le Bas (1999), Recurrent large-scale landsliding of the west flank of La Palma, Canary Islands, *J. Geophys. Res.*, *104*, 25,331–25,348.
- Vezzoli, L. (1988), Island of Ischia, *CNR Quaderni de La Ricerca Scientifica*, *114*(10), 122.
- Vincent, P. M., J. L. Bourdier, and G. Boudon (1989), The primitive volcano of Mount Pelée: Its construction and partial destruction by flank collapse, *J. Volcanol. Geotherm. Res.*, *38*(1), 1–15.
- Wadge, G., B. Voight, R. S. J. Sparks, P. D. Cole, S. C. Loughlin, and R. E. A. Robertson (2014), An overview of the eruption of Soufrière Hills Volcano, Montserrat from 2000 to 2010, in *The Eruption of the Soufrière Hills Volcano, Montserrat from 2000–2010, Memoirs of the Geological Society of London 3*, edited by G. Wadge, R. E. A. Robertson, and B. Voight, Geol. Soc. London Mem., *39*, 1–39.
- Wall-Palmer, D., et al. (2014), Late Pleistocene stratigraphy of IODP Site U1396 and compiled chronology offshore of south and south west Montserrat, Lesser Antilles, *Geochem. Geophys. Geosyst.*, *15*, 3000–3020, doi:10.1002/2014GC005402.
- Ward, S. N., and S. Day (2003), Ritter Island Volcano-lateral collapse and the tsunamis of 1888, *Geophys. J. Int.*, *154*, 891–902.
- Watt, S. F. L., et al. (2012a), Combinations of volcanic-flank and seafloor-sediment failure offshore Montserrat, and their implications for tsunami generation, *Earth Planet. Sci. Lett.*, *319*(320), 228–240, doi:10.1016/j.epsl.2011.11.032.
- Watt, S. F. L., et al. (2012b), Widespread and progressive seafloor-sediment failure following volcanic debris avalanche emplacement: Landslide dynamics and timing offshore Montserrat, Lesser Antilles, *Mar. Geol.*, *323*(325), 69–94, doi:10.1016/j.margeo.2012.08.002.
- Watts, A. B., and D. G. Masson (1995), A giant landslide on the north flank of Tenerife, Canary Islands, *J. Geophys. Res. Solid Earth*, *100*, B12, 24487–24498.
- Watt, S. F. L., P. J. Talling, and J. E. Hunt (2014), New insights into the emplacement dynamics of volcanic island landslides, *Oceanography*, *27*, 46–57.
- Weaver, P. P. E., R. G. Rothwell, J. Ebbing, D. Gunn, and P. M. Hunter (1992), Correlation, frequency of emplacement and source directions of megaturbidites on the Madeira Abyssal Plain, *Mar. Geol.*, *109*(1–2), 1–20.
- Wynn, R. B., D. J. W. Piper, and M. J. R. Gee (2002), Generation and migration of coarse-grained sediment waves in turbidity current channels and channel-lobe transition zones, *Marine Geology*, *192*(1), 59–78.
- Yoshida, H., T. Sugai, and H. Ohmori (2012), Size-distance relationships for hummocks on volcanic rockslide-debris avalanche deposits in Japan, *Geomorphology*, *136*(1), 76–87, doi:10.1016/j.geomorph.2011.04.044.